NASA Technical Memorandum 102509

Model Development in Viscoplastic Ratchetting

Alan D. Freed
Lewis Research Center
Cleveland, Ohio

and

Kevin P. Walker
Engineering Science Software, Inc.
Smithfield, Rhode Island

April 1990

NASA

MODEL DEVELOPMENT IN VISCOPLASTIC RATCHETTING

Alan D. Freed

NASA Lewis Research Center
Cleveland, OH 44135

Kevin P. Walker

Engineering Science Software, Inc.
Smithfield, RI 02917

ABSTRACT

Space Station Freedom's solar dynamic power modules, like all power plants, contain components that are subjected to conditions which favor thermally driven ratchetting. Existing viscoplastic models tend to overpredict ratchetting behavior, because their back stress (the kinematic variable) seems to "stick" more than it should during unloading. For this reason, a study has been undertaken to compare a variety of possible modifications to the evolution equation for back stress. All models considered herein have a hardening *vs.* dynamic-recovery format. To remove the stickiness of the back stress, a linear dependence on stress rate is introduced into the evolution equation for back stress in a variety of ways. Several favorable models have been screened out of the field of candidates by qualitatively determining their relative ability to fit experimentally observed behavior through six numerical experiments. A final selection must be made by quantitatively correlating the proposed models with experimental data, and then seeing which candidate does the best job of predicting observed ratchetting behavior. This is a subject of future work.

1. INTRODUCTION

Space Station Freedom (fig. 1) will be primarily powered by vast photovoltaic panels (75 kW total - phase I implementation). Under consideration as an option, supplemental power (two 25 kW units - phase II implementation) will be furnished through large solar reflectors (fig. 2) that will focus the Sun's energy into a solar receiver (fig. 3). The receiver of each solar dynamic power module is to be lined with 82 working fluid tubes, around each of which will be 96 canisters (fig. 4) manufactured from Haynes 188 - a cobalt alloy with good corrosion resistance and high-temperature strength. Contained within these canisters will be a phase change material (a $LiF\text{-}CaF_2$ eutectic salt) whose latent heat of solidification will be a source of thermal energy during periods of eclipse. The working fluid will transport this thermal energy to heat engines for electric power generation. The thermodynamic cycle of operation is the closed Brayton cycle.

A thermal analysis of the solar receiver determined that the maximum heat flux occurs at an axial location a little more than one meter from the aperture plate (fig. 3) [1]. The thermal history for a canister at this location is shown in idealized form in fig. 5. On coming out of eclipse, time zero in the figure, the salt is in solid form and the canister temperature is about 690°C at the location selected for detailed analysis. During the first 10 minutes or so, the temperature increases to a value of 767°C, at which point the salt starts to liquify. The peak temperature of the cycle, about 830°C, is reached after 54 minutes, at which time the space station goes into eclipse. Subsequently, the canister temperature drops quite rapidly to a value of 767°C, where the salt starts to solidify. The temperature remains constant there until the solidification process is completed, at about 80 minutes into the cycle. During the balance of the cycle, heat is rejected from the receiver with the salt in solid form. After 91 minutes, the space station comes out of eclipse and the cycle is repeated.

Using this idealized temperature history, an elastic analysis was performed to determine the maximum values of stress and strain introduced into the canister [1]. The von Mises equivalent stress obtained from this analysis is presented in idealized form in fig. 5, along with the thermal history. The predicted elastic stresses for the service cycle range between 22 and 50 MPa, with a cyclic mean stress of 36 MPa. More recently, the idealized thermomechanical stress/temperature/time history of fig. 5 was applied to a uniaxial test specimen to determine if this elastic analysis is adequate [2]. The resulting experimental stress-strain response (fig. 6) clearly illustrates that an elastic analysis is not adequate for this application, and an inelastic analysis needs to be conducted. A viscoplastic model is under development to perform this analysis, of which this paper presents progress made towards this goal. The inelastic response of fig. 6 also indicates that ratchetting (the accumulation of cyclic strain due to the presence of a mean stress) is an important feature to be modeled. The extent of ratchetting in fig. 6 is accentuated by the fact that this test was conducted in stress control, which is not indicative of the canister whose boundary conditions would probably be more closely approximated by a strain control test. Nevertheless, inelasticity is likely to exist; consequently, the potential of ratchetting is likely to exist, too. Vital questions to be answered by this analysis are: if ratchetting exists, will the ratchetting stop, *i.e.*, shakedown, or will it continue to accumulate over the life of the structure (30 years design life) possibly resulting in a premature failure; and if shakedown occurs, will a solar dynamic power module cold shut-down and restart reinitiate the ratchetting process? It is our hope to answer these questions in the near future.

Existing viscoplastic models tend to predict a material response that is too soft under ratchetting conditions, *i.e.*, they overpredict the cyclic strain accumulation in the presence of a mean stress. This modeling deficiency of viscoplasticity has received attention in the recent modeling efforts of MCDOWELL & LAMAR [3] and CHABOCHE [4]. The cause of this deficiency is ingrained within the hardening/dynamic-recovery format used for the evolution of back stress in most viscoplastic models. Simply put, this format results in a back stress that "sticks" during unloading more than it appears it should. Our basic objective here is to explore alternative formulations for the evolution of back stress that are physically acceptable, and which remove this stickiness. Our approach is to introduce terms that are linear in stress rate into the evolution equation for back stress, in accordance with LUBLINER's [5] thermodynamic theory with internal variables. This will enable the back stress to evolve more readily under conditions of unloading, thereby removing this undesired stickiness. Having the back stress evolve at rates that are first-order in stress rate results in an evolution equation that is a function of past histories *and* of present values of stress, and the formalism is within the scope of the memory-functional approach. Inclusion of higher-order stress rates would put it outside this scope [5], which is not acceptable.

2. EVOLUTION OF STRAIN

The strain ε_{ij} is taken to be the sum of an elastic strain ε^e_{ij} (including thermal strain) and an inelastic (or plastic) strain ε^p_{ij} such that

$$\varepsilon_{ij} = \varepsilon^e_{ij} + \varepsilon^p_{ij} \quad , \quad \varepsilon^p_{kk} = 0 \tag{1}$$

with no elastic or inelastic strain occurring in the stress-free virgin state. In this state, the material is taken to be isotropic. Small strains, displacements, and rotations in a Cartesian reference configuration are considered to make up the deformation history of the material. The trace of inelastic strain is zero valued implying plastic incompressibility. Repeated Latin indicies are summed over from 1 to 3 in the usual manner.

The constitutive equation governing elastic strain is that of classical thermoelasticity, and is given by

$$\varepsilon^e_{ij} = \frac{1+\nu}{E}\,\sigma_{ij} - \frac{\nu}{E}\,\sigma_{kk}\,\delta_{ij} + \alpha\,\Delta T\,\delta_{ij} \tag{2}$$

where E is the elastic modulus, ν is the Poisson ratio, α is the coefficient of thermal expansion, $\Delta T = T - T_0$ is the change in temperature with T_0 denoting the reference temperature, σ_{ij} is the stress, and δ_{ij} is the Kronecker delta. The elastic material constants for Haynes 188 are given in table 1.

The evolution equation for inelastic strain is taken to be of a form used previously by the authors [7], and is given by the differential equation

$$\dot{\varepsilon}^p_{ij} = \frac{3}{2}\,\theta\,Z\,\frac{S_{ij} - B_{ij}}{|S - B|} \tag{3}$$

with the back stress B_{ij} being composed of short- X_{ij} and long-range terms, *viz.*

$$B_{ij} = X_{ij} + \frac{2}{3} H_l \, \varepsilon^p_{ij} \tag{4}$$

and where the thermal diffusivity $\theta > 0$ is defined by [8]

$$\theta = \begin{cases} \exp\left[\dfrac{-Q}{kT}\right] & ; \quad \dfrac{T}{T_t} \geq 1 \\ \exp\left\{\dfrac{-Q}{kT_t}\left[\ln\left(\dfrac{T_t}{T}\right) + 1\right]\right\} & ; \quad \dfrac{T}{T_t} \leq 1 \end{cases} \tag{5}$$

and the Zener parameter $Z \geq 0$ is taken to be

$$Z = \frac{|\dot{\varepsilon}^p|}{\theta} = \left[\frac{|S - B|}{D}\right]^{mn} + \left[\frac{A}{A'}\right]^{n'} \left[\frac{|S - B|}{D}\right]^{mn'} \tag{6}$$

with norms (or magnitudes) defined by

$$|\dot{\varepsilon}^p| = \sqrt{(2/3)\dot{\varepsilon}^p_{ij}\dot{\varepsilon}^p_{ij}} \quad , \quad |J| = \sqrt{(3/2)J_{ij}J_{ij}} \tag{7}$$

where $J_{ij} \in \{S_{ij}, B_{ij}, X_{ij}, S_{ij}-B_{ij}\}$. The tensor $S_{ij} = \sigma_{ij} - \sigma_{kk}\delta_{ij}/3$ defines the deviatoric stress. The back (or internal) stress B_{ij} accounts for kinematic hardening behavior, whose short-range component is X_{ij}, and whose long-range component is $(2/3)H_l\varepsilon^p_{ij}$, where H_l is the long-range hardening modulus. The other material constants are: the activation energy Q, the transition temperature T_t, the power-law coefficients A and A' and exponents n and n', and the constant structure exponent m. The difference $S_{ij}-B_{ij}$ is the viscous stress (or overstress) that drives inelastic flow. The scalar D is the drag strength which is taken to be constant-valued herein, *i.e.*, no isotropic hardening is considered. A dot "$\cdot$" implies the time rate of change of its argument. The norms that are chosen scale the model for tension. The double power-law Zener parameter of eqn. 6 has been shown to apply for homologous temperatures (absolute temperature divided by melting temperature) exceeding about 0.25 [7], which is the case in this application (but not for the cold shut-down and restart problem). The inelastic material constants used in this study to qualitatively represent Haynes 188 are given in table 2.

Constant	Units	Value [6]
E	MPa	$233000 - 49.1T - 4.44\times10^{-2}T^2$
μ†	MPa	$91700 - 30.7T - 8.44\times10^{-3}T^2$
α	1/°C	$11.8\times10^{-6} + 6.26\times10^{-9}T - 1.40\times10^{-12}T^2$
† $\nu = E/2\mu - 1$		

TABLE 1
Elastic Constants for Haynes 188. T is in Degrees Centigrade.

Values for the inelastic constants were obtained as follows. A transition temperature of six-tenths the melting temperature (*i.e.* $T_t = 0.6T_m$, where $T_m \approx 1575$°K) was assumed, in accordance with the general observations of SHERBY & MILLER [9]. From steady-state creep rate data obtained above this transition temperature, an activation energy was determined using the relationship [10]

$$Q|_\sigma = k\left[\frac{1}{T_2} - \frac{1}{T_1}\right] \ln\left[\frac{\dot{\varepsilon}_1}{\dot{\varepsilon}_2}\right]_\sigma \tag{8}$$

where $\dot{\varepsilon}_1$ and $\dot{\varepsilon}_2$ are the steady-state creep rates associated with temperatures T_1 and T_2, respectively, at some fixed value of stress σ, and where k is the Boltzmann constant (8.314 J/mole°K). The steady-state Zener parameter given by [7]

$$Z_{ss} = \frac{|\dot{\varepsilon}^p|_{ss}}{\theta} = \left[\frac{|S|}{A}\right]^n + \left[\frac{|S|}{A'}\right]^{n'} \tag{9}$$

was then fit to experimental data from ref. 11 (see fig. 7) to determine values for the material constants A, A', n, and n'. The transient Zener parameter of eqn. 6 will reduce to the steady-state Zener parameter of eqn. 9 in the final model, wherein the limiting state of back stress L (defined in the next section) will be taken as a function of state rather than a constant (*cf.*, refs. 7 and 12). For the transient constants, H_l and H_s were given values of about 1/500 and 1/5 that of E, respectively, and m was given the value of 2, in accordance with rules of thumb established in ref. 7. Values for the drag strength D and the limiting state of back stress L were chosen so that predictions would roughly correlate with the saturated yield and ultimate strengths of this alloy, respectively.

Constant	Units	Value
A	MPa	0.0058
A'	MPa	0.94
D †	MPa	0.4
H_l †	MPa	35
H_s †	MPa	35000
L †	MPa	150
m †	-	2
n	-	3
n'	-	7
Q	J/mole	450000
T_t †	°K	945
† Actual value is unknown.		

TABLE 2
Inelastic Constants for Representation of Haynes 188.

The models presented in this report are sufficient to meet the report's primary objective, *viz.*, to study ratchetting behavior. A complete viscoplastic characterization of Haynes 188 will be presented in a future report. That model will include the effects of isotropic hardening and thermal recovery (among others), in addition to those effects modeled herein.

3. EVOLUTION OF BACK STRESS - SIX PRELIMINARY MODELS

To improve upon the capabilities of existing viscoplastic models in the description of ratchetting behavior, it seems to be necessary to remove the stickiness of the back stress during unloading. In most viscoplastic models, the back stress evolves with inelastic deformation only, which is virtually nonexistent during unloading; hence, the back stress sticks during unloading. The recent viscoplastic models of KREMPL *et al.* [13] and RAMASWAMY *et al.* [14], however, introduce an additional term into the evolution equation for back stress that is linear in stress rate, thereby removing this sticking characteristic which we deem to be a detriment. Such a linear term is admissible within the general thermodynamic constructs of LUBLINER [5]. The authors will provide a specific thermodynamic formulation for such a theory of viscoplasticity in a future report. Six equations for the evolution of the short-range back stress X_{ij} defined in eqn. 4 will now be considered. Their capabilities in producing desirable responses for several different loading histories are addressed in the following discussion section. Phenomenologically, the effect of the short-range back stress X_{ij} is to account for the initial transient curvature in an inelastic response, while the effect of the long-range back stress $(2/3)H_l\varepsilon^p_{ij}$ is to provide a linear strain-hardening response prevalent at the larger strains after the short-range back stress has saturated. It is the evolution of short-range back stress that is important in ratchetting problems, because it is the internal variable that most rapidly evolves after a load reversal.

Model A

A phenomenological description for the evolution of back stress used in most viscoplastic models was originally proposed by ARMSTRONG & FREDERICK [15], and has recently been derived from a dislocation slip theory by AIFANTIS [16], *i.e.*

$$\dot{X}_{ij} = \frac{2}{3} H_s \left\{ \dot{\varepsilon}^p_{ij} - \frac{3}{2} \frac{X_{ij}}{L} |\dot{\varepsilon}^p| \right\} \tag{10}$$

where H_s is the short-range hardening modulus and L is the limiting state of short-range back stress, both of which we take to be constants for the time being. The first term in the brackets represents a linear strain-hardening mechanism, while the second one represents a competing mechanism referred to as dynamic recovery. This relationship is used in most viscoplastic models for the evolution of back stress. It has been shown to be superior to a nonlinear Prager relationship, which employs a nonlinear strain-hardening mechanism without the aid of a competing dynamic recovery mechanism [7,12]. However, the Armstrong-Frederick model "sticks" during unloading producing an undesirable representation of ratchetting behavior [4].

Model B

This model replaces the plastic strain-rate terms in Model A with total strain-rate terms resulting in a hardening/recovery model akin to the original endochronic theory of viscoplasticity [17], *i.e.*

$$\dot{X}_{ij} = \frac{2}{3} H_s \left\{ \dot{e}_{ij} - \frac{3}{2} \frac{X_{ij}}{L} |\dot{e}| \right\} \tag{11}$$

where $e_{ij} = \varepsilon_{ij} - \varepsilon_{kk}\delta_{ij}/3$ is the deviatoric strain. Here the stress rate appears implicitly, since $\dot{e}_{ij} = \dot{S}_{ij}/2\mu + \dot{\varepsilon}^p_{ij}$ from eqns. 1 and 2, and where $\mu = E/2(1+\nu)$ is the elastic shear modulus. As a consequence, this model does not "stick" during unloading. Note that the dependence on stress rate appears in both the hardening and dynamic-recovery terms.

Model C

This model retains the tensorial nature (or directional characteristics) of Model A, while still introducing an effect due to stress rate, *i.e.*

$$\dot{X}_{ij} = \frac{2}{3} H_s \left\{ \frac{\dot{\varepsilon}^p_{ij}}{|\dot{\varepsilon}^p|} - \frac{3}{2} \frac{X_{ij}}{L} \right\} \left\{ |\dot{\varepsilon}^p| + \frac{|\dot{S}|}{E} \right\} \tag{12}$$

Like Model B, this model does not "stick" during unloading, and the stress rate is observed to influence both the hardening and dynamic-recovery terms.

Model D

This model combines the hardening term of Model B with the dynamic recovery term of Model A, *i.e.*

$$\dot{X}_{ij} = \frac{2}{3} H_s \left\{ \dot{e}_{ij} - \frac{3}{2} \frac{X_{ij}}{L} |\dot{\varepsilon}^p| \right\} \tag{13}$$

which does not "stick" during unloading, either. Here stress rate only affects hardening, not dynamic recovery, as in the viscoplastic models of KREMPL *et al.* [13] and RAMASWAMY *et al.* [14]. Except for the fact that H_s is a constant instead of a function, this is the evolution equation first proposed by Krempl and his colleagues. The model of Ramaswamy is also somewhat more general than that of eqn. 13, in that it allows some fixed percentage of elastic straining to influence hardening (*i.e.*, $\dot{\varepsilon}^p_{ij} + c_1 \dot{S}_{ij}/2\mu$ where $c_1 \in [0,1]$ is a constant, instead of $\dot{e}_{ij} \equiv \dot{\varepsilon}^p_{ij} + \dot{S}_{ij}/2\mu$).

Model E

Physically, it seems desirable that the back stress should not jump because of an imposed stress jump when at steady state (as in Model D). Thus, model E introduces a coefficient to the stress rate term that vanishes at saturation (because $|X| = L$ there) thereby satisfying this constraint, *i.e.*

$$\dot{X}_{ij} = \frac{2}{3} H_s \left\{ \dot{\varepsilon}^p_{ij} + \left[1 - \frac{|X|}{L} \right] \frac{\dot{S}_{ij}}{2\mu} - \frac{3}{2} \frac{X_{ij}}{L} |\dot{\varepsilon}^p| \right\} \tag{14}$$

However, this model "sticks" during unloading from a saturation state, just as Model A does. In fact, Models A and E are equivalent at saturation because the coefficient to the stress-rate term in eqn. 14 is zero-valued there.

Model F

An alternative representation that also restricts the back stress not to evolve in a stepwise manner from a stress jump when at steady state, and yet does not "stick" during unloading from saturation (as does Model E), is given by

$$\dot{X}_{ij} = \frac{2}{3} H_s \left\{ \dot{\varepsilon}^p_{ij} + \xi \frac{\dot{S}_{ij}}{2\mu} - \frac{3}{2} \frac{X_{ij}}{L} | \dot{\varepsilon}^p | \right\} \tag{15}$$

where

$$\xi = \left\{ \frac{3}{8} \left[\frac{S_{ij} - B_{ij}}{|S - B|} - \frac{X_{ij}}{L} \right] \left[\frac{S_{ij} - B_{ij}}{|S - B|} - \frac{X_{ij}}{L} \right] \right\}^{1/2} \tag{16}$$

is a scaling factor bound by the interval $0 \le \xi \le 1$. This variable defines a normalized distance between the current value of short-range back stress X_{ij} and its image point on the limit (or bounding) surface of radius L, in accordance with the theories of MROZ [18], DAFALIAS & POPOV [19] and MOOSBRUGGER & McDOWELL [20]. A graphic representation of this concept is presented in fig. 8. Here $n_{ij} = (3/2)(S_{ij} - B_{ij})/|S - B|$ is the unit vector establishing the direction of inelastic straining. The quantity $2L\xi\lambda_{ij} = (Ln_{ij} - (3/2)X_{ij})$ is the vector connecting the current value for the short-range back stress with its image point, where λ_{ij} is taken to be the unit vector. By determining the magnitude of $\xi\lambda_{ij}$ using $\sqrt{(2/3)\xi\lambda_{ij}\xi\lambda_{ij}}$, one obtains the expression for ξ given above. Note that what is referred to here as the image point is not the true image point associated with eqn. 15 (*cf.*, ref. 20), as it does not account for the stress rate term, but this is not a detriment for our application.

4. RATCHETTING EXPERIMENTS

The need for an accurate representation of ratchetting behavior is important for two reasons. First, ratchetting is an experimentally observed phenomenon that can dominate the observed response under certain boundary conditions; typically, cyclic loading in the presence of a mean stress. Second, there can be an unwanted theoretical artifact (a false ratchetting) that is not characteristic of observations; for example, when a small cycle (*e.g.*, the solar dynamic receiver cycle of fig. 5) is repeated and contained within a larger cycle (*i.e.*, the cold shut-down and restart cycle of the solar dynamic power module). Several experimental results obtained from a variety of materials are presented below to illustrate these two types of ratchetting behavior.

Typically, ratchetting is thought of as the cycle dependent accumulation of inelastic strain under stress-like boundary conditions brought about by the presence of a mean stress (*i.e.*, cyclic creep), where the direction of ratchetting is coaxial with that of the mean stress. For repeated loadings, this type of ratchet strain exponentially decays with cycling to a shakedown condition that is dependent on mean stress, provided that this mean stress is less than some threshold value; otherwise, ratchetting of this type continues to accumulate in an unstable manner to certain destruction. The experimental data of CHABOCHE [4] (presented here in fig. 9 for type 316 L stainless steel) illustrate these features of ratchetting. Ratchetting can also occur under strain-like boundary conditions resulting in a cyclic relaxation response. Cyclic relaxation, like cyclic creep, exponentially decays with cycling to a shakedown condition which also depends on the level of mean stress; fortunately, cyclic relaxation, unlike cyclic creep, cannot become unstable. The room temperature experimental data of KREMPL & KALLIANPUR [21] (presented here in fig. 10a for Ti-7Al-2Cb-1Ta) and the in-phase thermomechanical data of SWANSON *et al.* [22] (presented here in fig. 10b for PWA 1480 in the <001> orientation) illustrate these features of ratchetting.

A ratchetting response may be artifically produced by a viscoplastic theory when modeling a variable amplitude cyclic loading history [3,4]. If this type of history is prevalent in a given application (which it will be for the solar dynamic power modules, provided that they go through shut-down and restart cycles), then the viscoplastic theory to be used must address this potential problem to ensure meaningful predictions. To demonstrate how a false ratchetting response might come about, consider the room temperature data of CHABOCHE [4] (presented here in fig. 11a for type 316 L stainless steel) and the 950°C experimental data of NOUAILHAS & FREED [23] (presented here in fig. 11b for CMSX-2 in the <011> orientation) where smaller hysteresis loops are contained within a larger one. The stainless steel response in fig. 11a is representative of how most (but not all) materials behave; that is, there is closure of the smaller loop at the point of connection with the larger loop, independent of whether the smaller excursion is elastic or inelastic. This is a result that existing viscoplastic theories cannot predict, in general (with the one exception of the recent theory by McDOWELL & LAMAR [3]). The single crystal response in fig. 11b is not a typical material response, but nevertheless, it does occur for some

materials. Here closure does not exist for the smaller inelastic loops (but it does for elastic ones), which is a characteristic that viscoplastic theories can predict. Consequently, if this inner loop is repeated, then a ratchetting response (either cyclic creep or relaxation) would be predicted using existing technology. For the majority of materials, those that exhibit closure like type 316 L stainless steel, such a prediction would not be representative of actual material response; however, an accurate description would be predicted for those materials that do not exhibit closure, like CMSX-2. Whether or not Haynes 188 has this property of closure is presently unknown. If it does, which is probably the case, then features from the McDOWELL & LAMAR [3] theory will need to be incorporated.

There is one additional experimental result presented, which is not a ratchetting experiment, but rather, a strian-rate sensitivity experiment. Strain-rate sensitivity is the most fundamental characteristic of viscoplasticity. Figure 12 presents experimental data from KREMPL [24] for type 304 stainless steel where step jumps in the controlling strain-rate occur. Over the past decade, he and his students have performed similar experiments on a variety of materials, and all exhibit the same basic response. For any given strain rate, there exists a unique stress-strain curve. If there is a jump in strain rate, then there is an accompanying jump is stress to the appropriate stress-strain curve. Of course, where this curve resides in stress-strain space depends upon the history of deformation.

5. DISCUSSION OF SIX MODELS

To assess the relative merit of the six evolutionary models in §3 for their representation of ratchetting and other viscoplastic characteristics, six different numerical experiments have been performed on each model. The results are qualitative (*i.e.*, comparisons are made between trends in the data predicted by the six models) rather than quantitative (*i.e.*, comparisons being made between experimental data and predictions). This allowed the same values for the material constants to be used in all the calculations. Our assessment as to their relative merit in predicting appropriate trends is given in table 3.

EXPERIMENT	MODEL					
	A	B	C	D	E	F
1	U	Q	U	A	A	Q
2	A	U	U	A	A	A
3	A	U	U	A	A	A
4	Q	Q	U	A	A	A
5	U	U	U	U	U	U
6	A	A	A	Q	A	A

TABLE 3
Model Assessment. "A" is Acceptable. "Q" is Questionable. "U" is Unacceptable.

In all the predictions presented in this paper, both the stress and the back stress are plotted against strain. Many times the stress *vs.* strain response is quite similar between various model predictions for a given experiment, but the back stress *vs.* strain responses are vastly different. The back stress response therefore provides insight into a model's behavior that has meaning (albeit, intuitive for the most part) to the viscoplastician. There are but only a few experimental data sets which characterize the evolution of back stress. One such example is presented in fig. 13 from TRAMPCZYNSKI's [25] study of 18G2A streel at room temperature, where an unloading/reloading method was used to measure back stress. For both monotonic and cyclic conditions, the back stress response was observed to have a shape similar to that of the stress response.

The first experiment is a classical ratchetting test at 750°C, *i.e.*, cyclic creep. Stress is controlled at a rate of ±50 MPa/s over a stress range of -100 to 200 MPa with a mean stress of 50 MPa. The predictions given in fig. 14 are rated according to the following criteria. The prediction is acceptable if the rate of ratchetting diminishes with each successive cycle, as in Models D and E. It is rated questionable if this rate dimishes over a few cycles before going into a condition of steady state, as in Models B and F. And it is taken to be unacceptable if steady-state ratchetting occurs throughout the deformation history, as in Models A and C. In all fairness, Models A and F are softer than the others (a consequence of using the same values for the material constants in all calculations), and will therefore ratchet more than the other models do. This softness can be gauged by comparing

the inelastic strain ranges of the first cycle. Models A and F have about twice the inelastic strain range of the other models in the first cycle of loading.

The second experiment is an interrupted tensile test in strain control at 750°C. The uniaxial loading is to 0.01 strain, unloading to 0.0085 strain (approximately zero stress), and then followed by a reloading to 0.02 strain. The strain rate is ±0.001/s throughout. The predictions are presented in fig. 15. The desired result is elastic unloading with elastic reloading up to the flow stress at which unloading occurred, and then followed by a sharp transition to inelasticity with roughly the same tangent modulus as observed just prior to unloading. Models A, D, E and F give the desired response. A common feature shared by the models that do not produce the desired response, Models B and C, is that they both include an effect due to stress rate in the dynamic recovery term. As a result, there is too much unsticking of the back stress during unloading.

The third experiment is one of elastic ratchetting (*i.e.*, cyclic relaxation) under conditions of strain control at 750°C. Tensile preloading is to 0.01 strain, followed by 5 cycles of loading between 0.009 and 0.01 strain (at approximately 175 MPa mean stress). The strain rate is ±0.001/s throughout. The predictions are presented in fig. 16. The desired result is a condition of elastic ratchetting with a small (almost unmeasurable) amount of viscous stress relaxation that exponentially decays; however, the back stress should not relax. Again, Models A, D, E and F give the desired response, while Models B and C do not (for the same reason they did not do well in experiment 2). The difference in ratchetting rates observed in the predictions of Models B and C has to do with the fact that the inelastic strain- and stress-rate drivers can add or compete against each other in Model B, whereas they always add in Model C.

The fourth experiment is the first five cycles of an in-phase thermomechanical fatigue test, *i.e.*, another case of cyclic relaxation. The controlling mechanical strain rate is 0.001/s with a mechanical strain range of ±0.001. The temperature varies linearly in time over a range of 600 to 900°C. The predictions are presented in fig. 17. The desired response contains inelastic deformation during the first quarter cycle with a largely elastic response thereafter. A small amount of viscous stress relaxation is expected, as in experiment 2, but the back stress should not ratchet. Models D, E and F give a desirable response. Model C exhibits excessive ratchetting. Model B is questionable in that the back stress ratchets to a small degree. Model A is questionable only because it immediately attained a fully reversed condition with a small inelastic strain range showing no tendency of cyclic relaxation.

The fifth experiment is a large hysteresis loop containing two smaller loops inside it. The test is in strain control at a strain rate of ±0.001 throughout, and the temperature is 750°C. The tensile loading is to 0.01 strain, with unloading to -.005 strain, reloading to 0 strain, unloading to -.01 strain, reloading to 0.005 strain, unloading to 0 strain, and then reloading back to 0.01 strain. The predictions are presented in fig. 18, where the initial tensile loadings are not shown to keep the figures clean. The desired result is a symmetric outer loop which contains two symmetric inner loops that exhibit closure (or near closure) at the point of intersection with the outer loop. None of these models produces closure, and most do not produce symmetric inner loops. The inability of current viscoplastic models to produce this type of closure is discussed in refs. 3 and 4.

The sixth and final experiment is a tensile strain-rate jump test at 750°C for characterizing strain-rate sensitivity. The controlling strain rates are 0.01/s and 0.00001/s. The tensile loading is to 0.005 strain at the slower rate, then to 0.01 strain at the faster rate, then to 0.015 at the slower rate, and finally to 0.02 at the faster rate. The predictions are presented in fig. 19. All the models, except Model D, produce a desirable result in that the stress tracks a *master* curve indicative of the controlling strain rate. In Model D, the back stress jumps significantly caused by the accompanying stress jumps. This results in a questionable overshoot of stress when the back stress has saturated. The other models do not exhibit such significant jumps in back stress, nor do they cause an overshoot in stress due to a stress jump when the back stress has previously saturated.

In summary, Models D, E and F seem to be reasonable candidates for further study as improvements over Model A in the represention of ratchetting behavior. Models B and C are definitely unacceptable candidates for further study. We continue our study, in part, in the remaining sections of this report.

6. EVOLUTION OF BACK STRESS - FOUR ADDITIONAL MODELS

In the two-surface theories of plasticity [19], the tangent modulus is taken to be a function of the distance from the current value of stress on the yield surface to its image point on the limit surface, similar to our definition of ξ in eqn. 16 (see fig. 8). Considering a viscoplastic model like ours (with short- and long-range

components of back stress, where the long-range component is proportional to inelastic strain), MOOSBRUGGER & MCDOWELL [20] have demonstrated that a positive monotonically-decreasing function $H_s(\xi)$ for the hardening modulus (the analog to the tangent modulus of plasticity) in one evolution equation for short-range back stress does a better job of correlating nonproportional experimental data than do the more extensive viscoplastic models of CHABOCHE & ROUSSELIER [26] with two and three short-range back stresses whose hardening moduli are constant valued. The introduction of a hardening function $H_s(\xi)$ associated with one component of short-range back stress is a simple way to approximate the more accurate description of a large number of back stresses (say $n \gg 1$) whose hardening moduli are all constant valued, *i.e.*, it simulates a distribution of back stresses with different characteristic times. The result is a stress-strain response that is more smooth than what is observed in figs. 14 to 19, especially around the knee of the curve. KREMPL *et al.* [13] use a hardening function $H_s(|S-B|)$ which has the same overall effect; however, its application to nonisothermal conditions does not appear to us to be as straight forward.

In the four equations that follow for the evolution of short-range back stress, the hardening modulus in each is taken to be of the form

$$H_s(\xi) = c_3 + (c_2 - c_3)\,\xi \tag{17}$$

where $c_2 \geq c_3 > 0$ are constants. Both Krempl and McDowell use exponential forms, which may in fact be more physically correct. We choose a linear form here strictly for simplicity. In actual applications, it seems profitable to raise ξ to a power in eqn. 17, and to choose $c_2 \simeq E$ and $c_3 \simeq H_I$.

The four evolution equations that are considered can be represented by the single relationship, *i.e.*

$$\dot{X}_{ij} = \frac{2}{3} H_s(\xi) \left\{ \dot{\varepsilon}^p_{ij} + C \frac{\dot{S}_{ij}}{2\mu} - \frac{3}{2} \frac{X_{ij}}{L} |\dot{\varepsilon}^p| \right\} \tag{18}$$

where only the function C varies between the four models.

Model I

This model is of the form used by MOOSBRUGGER & MCDOWELL [20], which is a generalization of the Armstrong-Frederick model, Model A, *i.e.*

$$C = 0 \tag{19}$$

The following three models contain this one as a special case (*i.e.*, $c_1 = 0$).

Model II

This model is similar in form to the one used by KREMPL *et al.* [13], *i.e.*

$$C = \begin{cases} 0 \;, & |X| \geq L \;\text{ and }\; (S_{ij} - B_{ij})\dot{S}_{ij} \geq 0 \\ c_1 \;, & \text{else} \end{cases} \tag{20}$$

where $c_1 \in [0,1]$ is a constant. This is a generalization of Model D where the switch on C is added to refrain the short-range back stress from taking on values outside of its bounding surface (see fig. 8). This eliminates the overshooting exhibited by Model D in fig. 19.

Model III

This model is a generalization to Model E, *i.e.*

$$C = c_1 \left[1 - \frac{|X|}{L} \right] \tag{21}$$

where $c_1 \in [0,1]$ is a constant.

Model IV

This model is a generalization to Model F, *i.e.*

$$C = c_1 \xi \tag{22}$$

where $c_1 \in [0,1]$ is a constant, and ξ is the variable defined in eqn. 16.

7. DISCUSSION OF FOUR MODELS

These four models are used to predict the same six numerical experiments that the previous six models were used to predict. Values used for the additional material constants are presented in table 4. Our assessment of the capability of Models I to IV to predict reasonable responses for these six experiments is presented in table 5.

Constant	Units	Value
c_1	-	1.0
c_2	MPa	0.99 E
c_3	MPa	0.1 E

TABLE 4
Additional Inelastic Constants.

EXPERIMENT	MODEL			
	I	II	III	IV
1	U	A	A	Q
2	Q	A	A	A
3	A	A	A	A
4	A	A	A	A
5	U	U	U	U
6	A	A	A	A

TABLE 5
Model Assessment. "A" is Acceptable. "Q" is Questionable. "U" is Unacceptable.

For the stress-controlled ratchetting experiment (*no.* 1) presented in fig. 20, the same rating scale is used as was used for the data of fig. 14. Model I is unacceptable (as was Model A) because a steady-state ratchetting condition exists from the very onset of the deformation history. Models II and III predict a transient decay in the rate of ratchet strain accumulation, and are therefore acceptable. Model IV has a transient ratchetting response that becomes a steady-state response after a few cycles, and is therefore taken to be a questionable prediction. Again, in all fairness, Models I and IV are much softer than Models II and III (a consequence of using the same material constants for all the models) and therefore should ratchet more for this experiment.

For experiment 2, only Model I does not produce a desirable result, as seen in fig. 21. The yield stress upon reloading does not match the prior flow stress at unloading. This is curious since its counterpart, Model A, does give a good representation of observed behavior for this experiment (see fig. 15).

All four models provide a reasonable description for experiment 3, as shown in fig. 22. This is not suprising, since their four counterparts - Models A, D, E and F - also do well in representing this experiment.

All four models produce acceptible results for the themomechanical test (experiment 4), as shown in fig. 23.

The predictions of the smaller loops inside the larger hysteresis loop of experiment 5 (see fig. 24) are not representative of typical material behavior for the same reason as before - closure of the smaller loops does not exist. However, there is some improvement in the predictions of these models over those of the first set. Of these four models, Models I, II and IV produce the best shape (symmetry) of the inner loops. It is not known what influence the nonlinear hardening function $H_s(\xi)$ has on closure properties for this particular experiment.

All four predicted responses of the strain-rate jump experiment (*no.* 6) presented in fig. 25 are in accordance with experimental observations. Introducing the switch into Model II (eqn. 20) removes the stress overshoots of Model D observed in fig. 19. This switch may not be necessary if c_3 in eqn. 17 is sufficiently

small.

8. CONCLUSIONS

Current viscoplastic models are known to overpredict ratchetting phenomena; a result of the back stress "sticking" too much during unloading. The need to be able to accurately predict ratchetting behavior over long periods of time is recognized as an important concern in the design of Space Station Freedom's solar dynamic receiver. In order to remove this stickiness, terms that are linear in stress rate have been incorporated into the evolution equation of the short-range back stress. Ten different models have been studied. In order to assess their relative merit, six different numerical experiments have been performed on each model. The following conclusions are drawn from this study.

1) The introduction of a term that is linear in stress rate is a viable way to alleviate sticking of the back stress during unloading.

2) Within a hardening/dynamic-recovery format, only the hardening term should have a stress-rate dependence.

3) A positive monotonic-decreasing function $H_s(\xi)$ for the hardening modulus of short-range back stress produces a superior response to that of a constant-valued hardening modulus.

4) Of the models considered, Models II, III and IV seem to be the most capable. The authors prefer Models II and IV over the others for physical reasons. Which model does the best job of correlating actual data is a subject of future work.

5) Altering the value of $c_1 \in [0,1]$ in Models II, III and IV directly influences the degree of ratchetting that they predict, with the limiting case of $c_1 = 0$ resulting in a classical Armstrong-Frederick model, *i.e.*, Model I, which is known to overperdict ratchetting phenomena.

REFERENCES

[1] Tong, M. T., Kerslake, T. W., and Thompson, R. L., "Structural Assessment of a Space Station Solar Dynamic Heat Receiver Thermal Energy Storage Canister," AIAA Paper No. 88-2487, Proceedings of the Conference: *AIAA SDM Issues of the International Space Station*, Williamsburg, VA, April 21-22, 1988, pp. 162-172.

[2] Ellis, J. R., Bartolotta, P. A., and Mladsi, S. W., "Preliminary Study of Creep Thresholds and Thermomechanical Response in Haynes 188 at Temperatures in the Range 649 to 871°C," *Turbine Engine Hot Section Technology 1987*, NASA CP-2493, 1987, pp. 317-334.

[3] McDowell, D. L., and Lamar, A. B., "Modeling Ratchetting and Anisotropic Deformation with Hardening Dynamic Recovery Format Models," *Advances in Plasticity 1989*, eds. A. S. Khan and M. Tokuda, Pergamon Press, 1989, pp. 247-251.

[4] Chaboche, J.-L., "On Some Modifications of Kinematic Hardening to Improve the Description of Ratchetting Effects," to appear in: *Int. J. Plast.*, 1989.

[5] Lubliner, J., "On the Structure of the Rate Equations of Materials with Internal Variables," *Acta Mech.*, Vol. 17, 1973, pp. 109-119.

[6] Bonacuse, P. J., and Kalluri, S. R., private communication, NASA - Lewis Research Center, 1989.

[7] Freed, A. D., and Walker, K. P., "Refinements in a Viscoplastic Model", *NASA TM-102338*, 1989.

[8] Miller, A., "An Inelastic Constitutive Model for Monotonic, Cyclic, and Creep Deformation: Part I, Equations Development and Analytical Procedures," *J. Eng. Mater. Technol.*, Vol. 98, 1976, pp. 97-105.

[9] Sherby, O., and Miller, A. K., "Combining Phenomenology and Physics in Describing the High Temperature Mechanical Behavior of Crystalline Solids," *J. Eng. Mater. Technol.*, Vol. 101, 1979, pp. 387-395.

[10] Sherby, O. D., and Burke, P. M., "Mechanical Behavior of Crystalline Solids at Elevated Temperature," *Progress in Materials Science*, Vol. 13, eds. B. Chalmers and W. Hume-Rothery, Pergamon Press, 1968, pp. 325-390.

[11] Materials Data Book for Haynes Alloy No. 188, Cabot Corp., 1983.

[12] Freed, A. D., "Thermoviscoplastic Model With Application to Copper," *NASA TP-2845*, 1988.

[13] Krempl, E., McMahon, J. J., and Yao, D., "Viscoplasticity Based on Overstress With a Differential Growth Law for the Equilibrium Stress," *Mech. Materl.*, Vol. 5, 1986, pp. 35-48.

[14] Ramaswamy, V. G., Van Stone, R. H., Dame, L. T., and Laflen, J. H., "Constitutive Modeling for Isotropic Materials," *NASA CR-175004*, 1985.

[15] Armstrong, P. J., and Frederick, C. O., "A Mathematical Representation of the Multiaxial Bauschinger Effect," *CEGB RD/B/N731*, Berkeley Nuclear Laboratories, 1966.

[16] Aifantis, E. C., "The Physics of Plastic Deformation," *Int. J. Plast.*, Vol. 3, 1987, pp. 211-247.

[17] Valanis, K. C., "A Theory of Viscoplasticity Without a Yield Surface: Part I, General Theory," *Arch. Mech.*, Vol. 23, 1971, pp. 517-533.

[18] Mróz, Z., "On the Description of Anisotropic Workhardening," *J. Mech. Phys. Solids*, Vol. 15, 1967, pp. 163-175.

[19] Dafalias, Y. F., and Popov, E. P., "A Model of Nonlinearly Hardening Materials for Complex Loading, *Acta Mech.*, Vol. 21, 1975, pp. 173-192.

[20] Moosbrugger, J. C., and McDowell, D. L., "On a Class of Kinematic Hardening Rules for Nonproportional Cyclic Plasticity," *J. Eng. Mater. Technol.*, Vol. 111, 1989, pp. 87-98.

[21] Krempl, E., and Kallianpur, V. V., "The Uniaxial Unloading Behavior of Two Engineering Alloys at Room Temperature," *J. Appl. Mech.*, Vol. 52, 1985, pp. 654-658.

[22] Swanson, G. A., Linask, I., Nissley, D. M., Norris, P. P., Meyer, T. G., and Walker, K. P., "Life Prediction and Constitutive Models for Engine Hot Section Anisotropic Materials Program," *NASA CR-179594*, 1987.

[23] Nouailhas, D., and Freed, A. D., "A Viscoplastic Theory for Anisotropic Materials," submitted to: *J. Eng. Mater. Technol.*

[24] Krempl, E., "Models of Viscoplasticity: Some Comments on Equilibrium (Back) Stress and Drag Stress," *Acta Mech.*, Vol. 69, 1987, pp. 25-42.

[25] Trampczynski, W., "The Experimental Verification of the Evolution of Kinematic and Isotropic Hardening in Cyclic Plasticity," *J. Mech. Phys. Solids*, Vol. 36, 1988, pp. 417-441.

[26] Chaboche, J.-L, and Rousselier, G., "On the Plastic and Viscoplastic Constitutive Equations: Part I, Rules Developed With Internal Variable Concept," *J. Pressure Vessel Technol.*, Vol. 105, 1983, pp. 153-158.

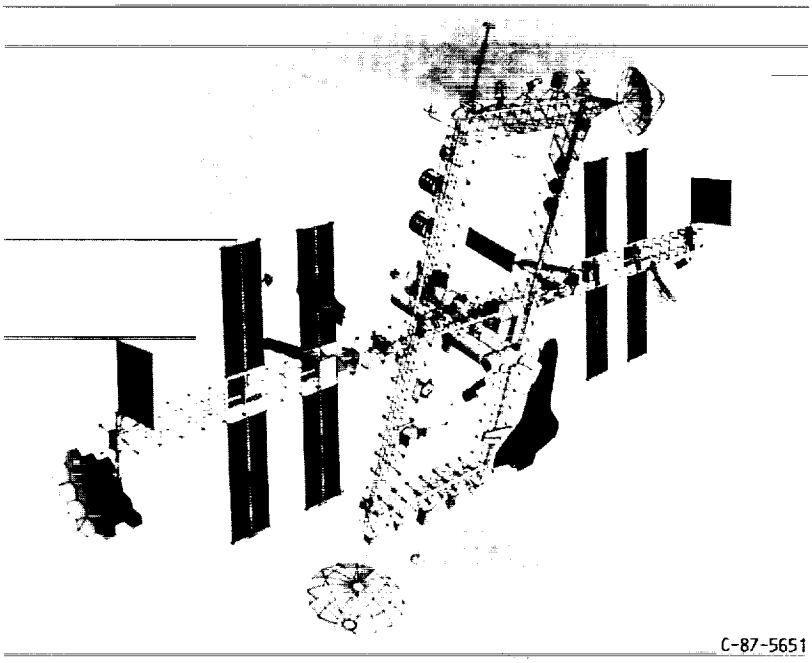

FIGURE 1. - SPACE STATION FREEDOM - PHASE II CONFIGURATION.

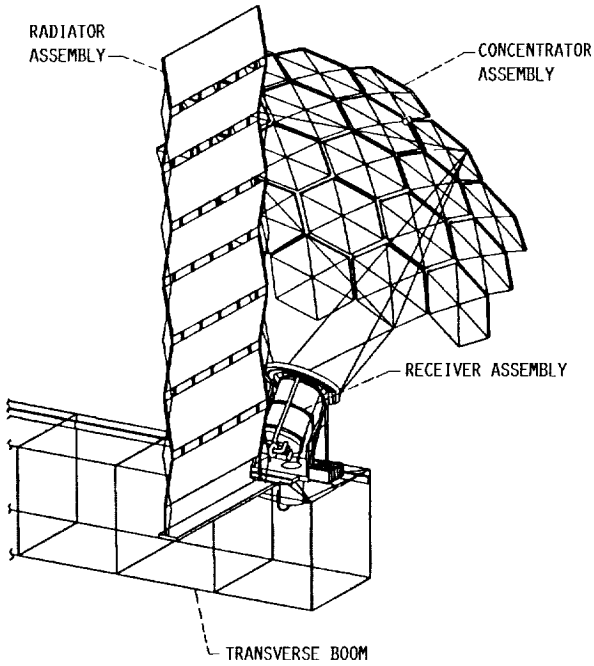

FIGURE 2. - CLOSED BRAYTON CYCLE SOLAR DYNAMIC POWER MODULE.

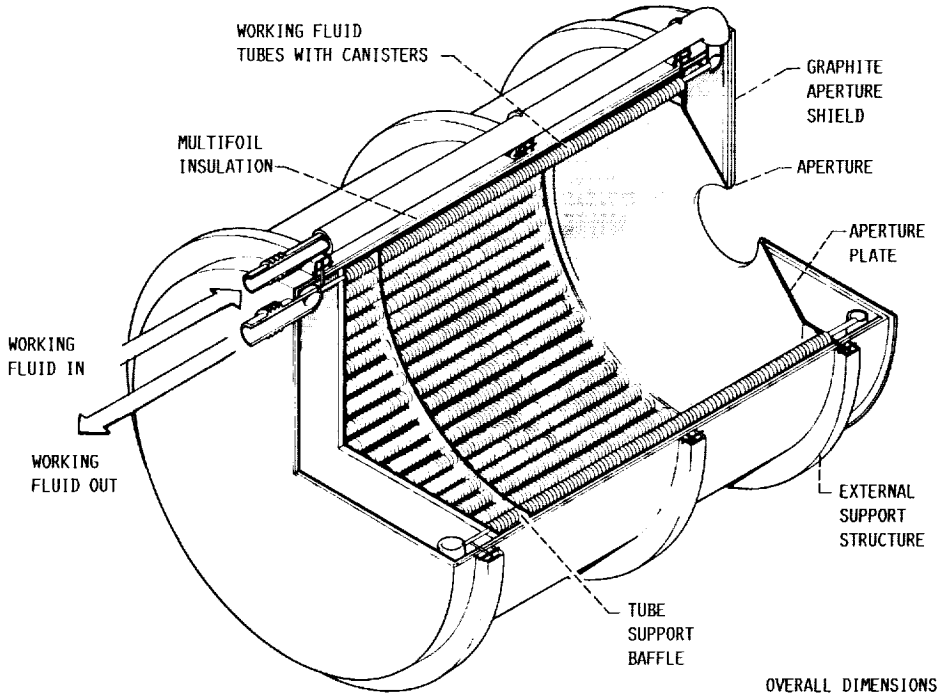

FIGURE 3. - SPACE STATION SOLAR RECEIVER.

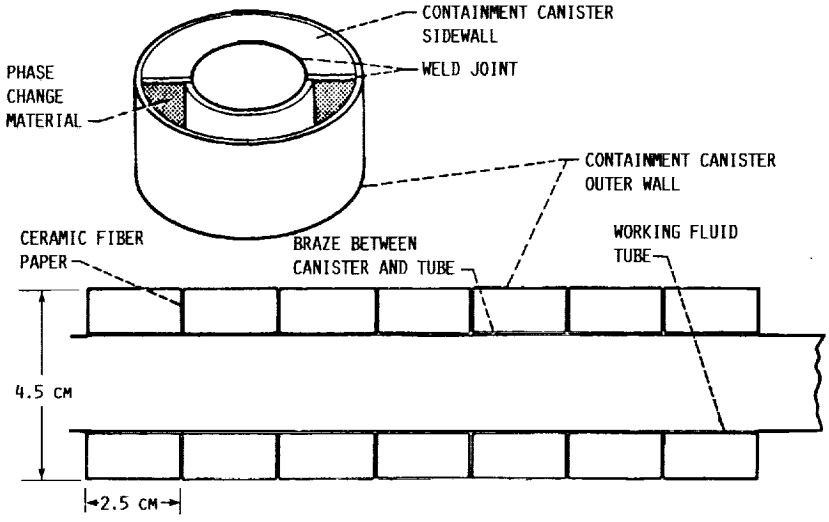

FIGURE 4. - SOLAR RECEIVER WORKING FLUID TUBE AND CANISTER CONFIGURATION.

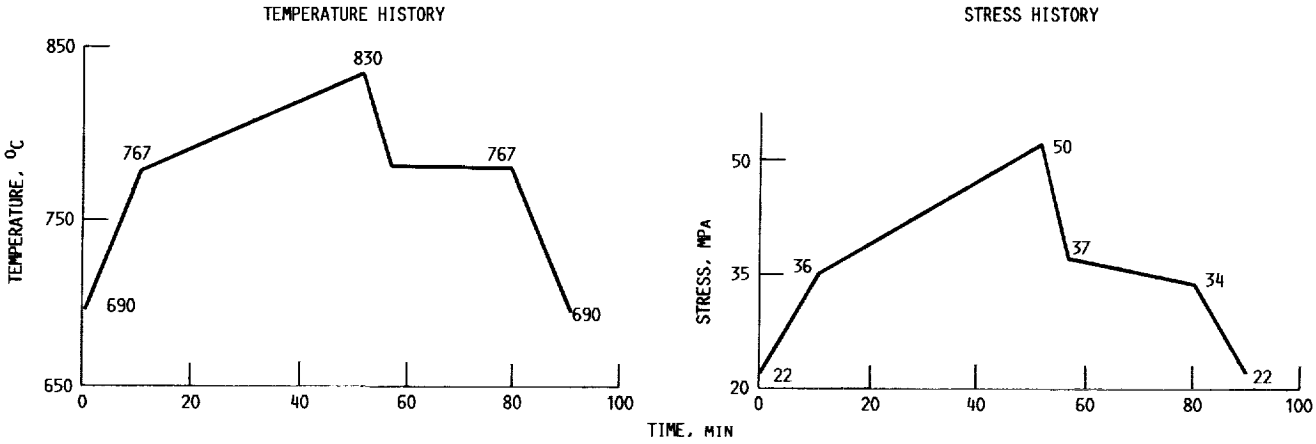

FIGURE 5. - THERMOMECHANICAL HISTORY OF CANISTER AT LOCATION OF MAXIMUM HEAT FLUX.

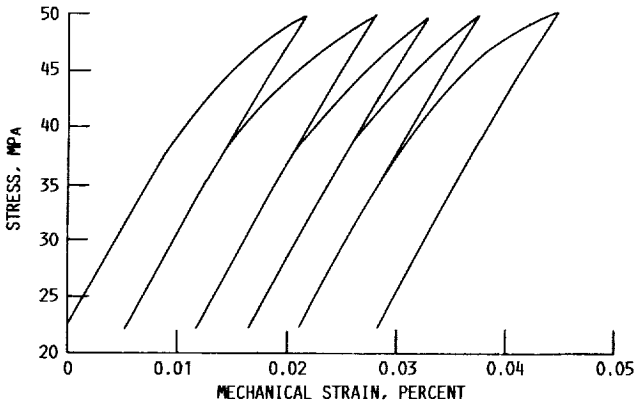

FIGURE 6. - EXPERIMENTAL RESPONSE OF HAYNES 188 TO 5 LOADING CYCLES OF THE STRESS/TEMPERATURE HISTORY IN FIGURE 5.

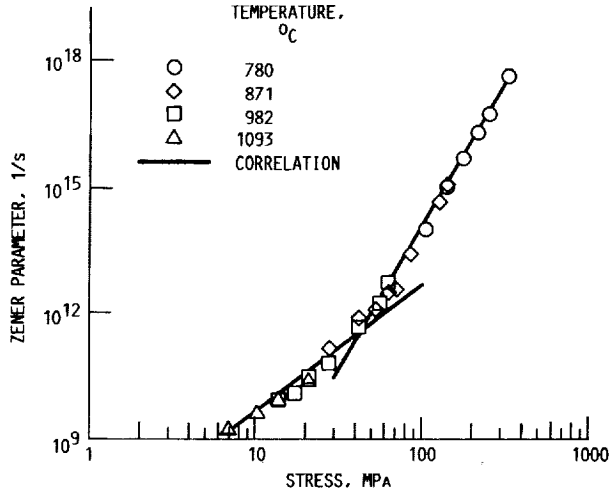

FIGURE 7. - STEADY-STATE CREEP RESPONSE OF HAYNES 188. (DATA FROM REF. 11). Q = 450 000 J/MOLE; A = 0.0058 MPA; A' = 0.94 MPA; n = 3; n' = 7.

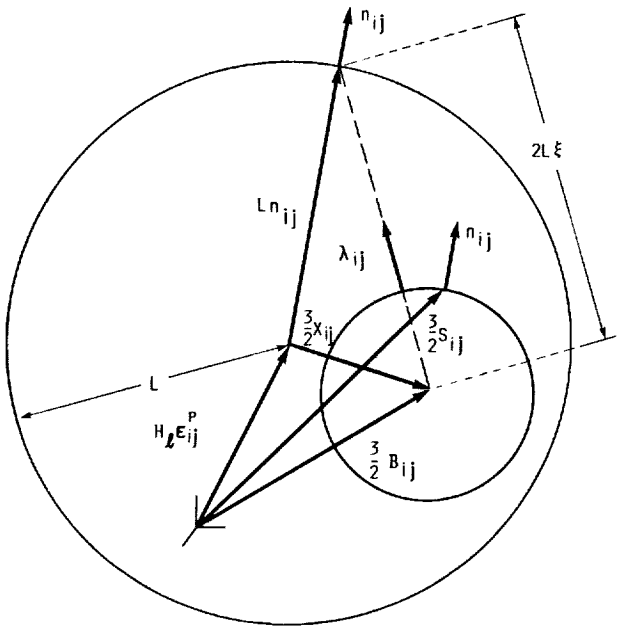

FIGURE 8. - IMAGE POINT OF SHORT-RANGE BACK STRESS.

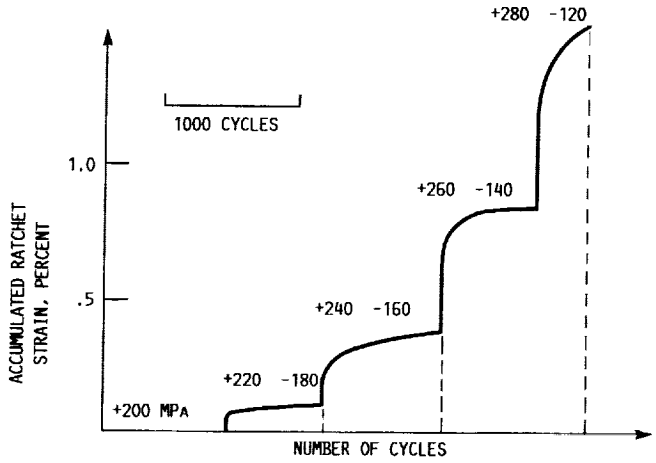

FIGURE 9. - RATCHET RESPONSE OF TYPE 316 L STAINLESS STEEL AT ROOM TEMPERATURE UNDER STRESS CONTROL. (DATA ARE FROM REF. 4).

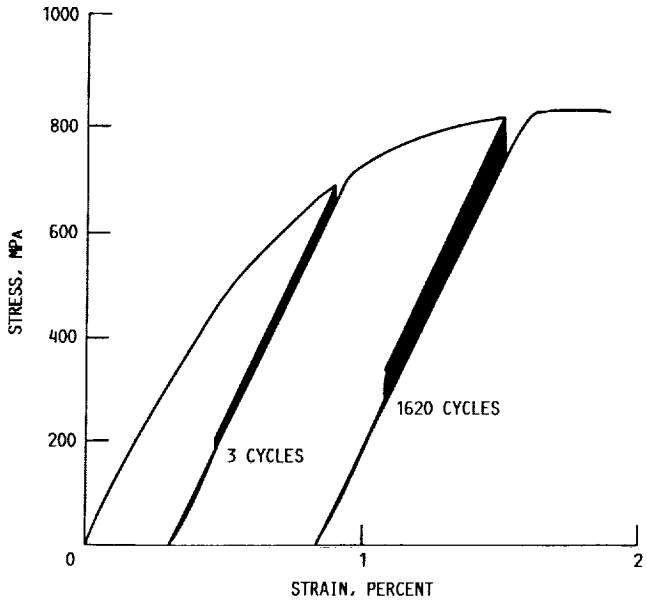

(a) Ti-7Al-2Cb-1Ta AT ROOM TEMPERATURE.

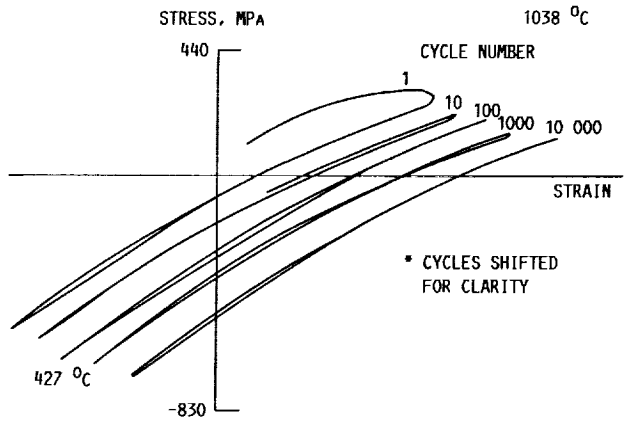

(b) PWA 1480 IN <001> ORIENTATION UNDER IN-PHASE THERMOMECHANICAL LOADING. STRAIN AMPLITUDE IS ±0.004.

FIGURE 10. - RATCHET RESPONSE UNDER STRAIN CONTROL. (DATA ARE FROM REF. 21 AND 22, RESPECTIVELY).

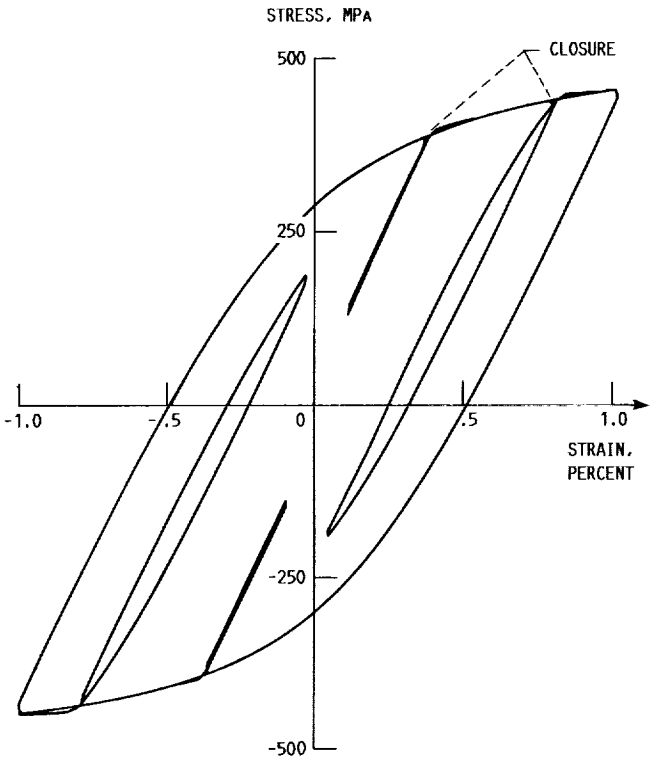

(a) TYPE 316 L STAINLESS STEEL AT ROOM TEMPERATURE.

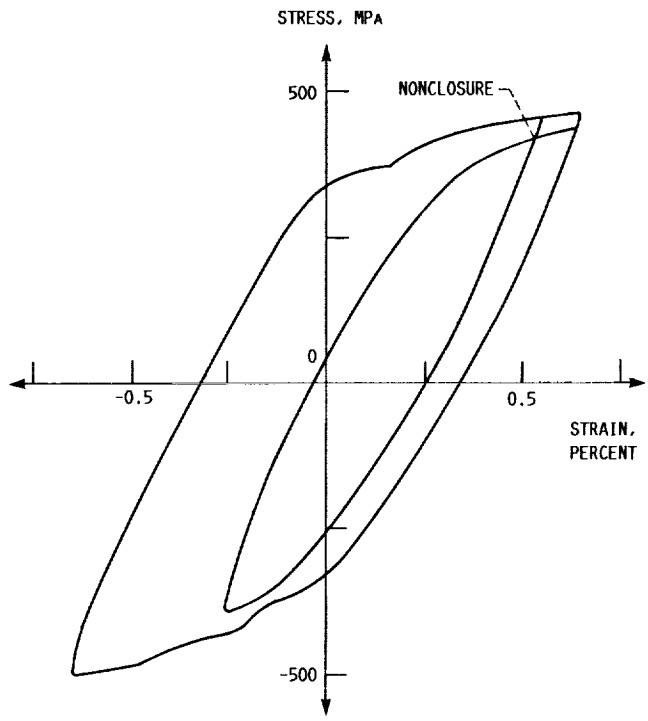

(b) CMSX-2 IN <011> ORIENTATION AT 950 ^{o}C.

FIGURE 11. - SMALL LOOP CLOSURE BEHAVIOR. (DATA ARE FROM REF. 4 AND 23, RESPECTIVELY).

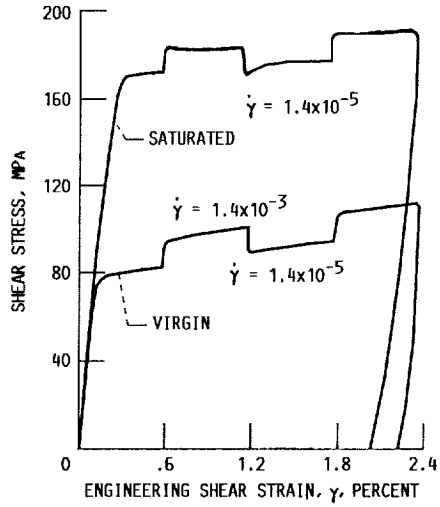

FIGURE 12. - STRAIN-RATE SENSITIVITY OF TYPE 304 STAINLESS STEEL AT ROOM TEMPERATURE. (DATA ARE FROM REF. 24).

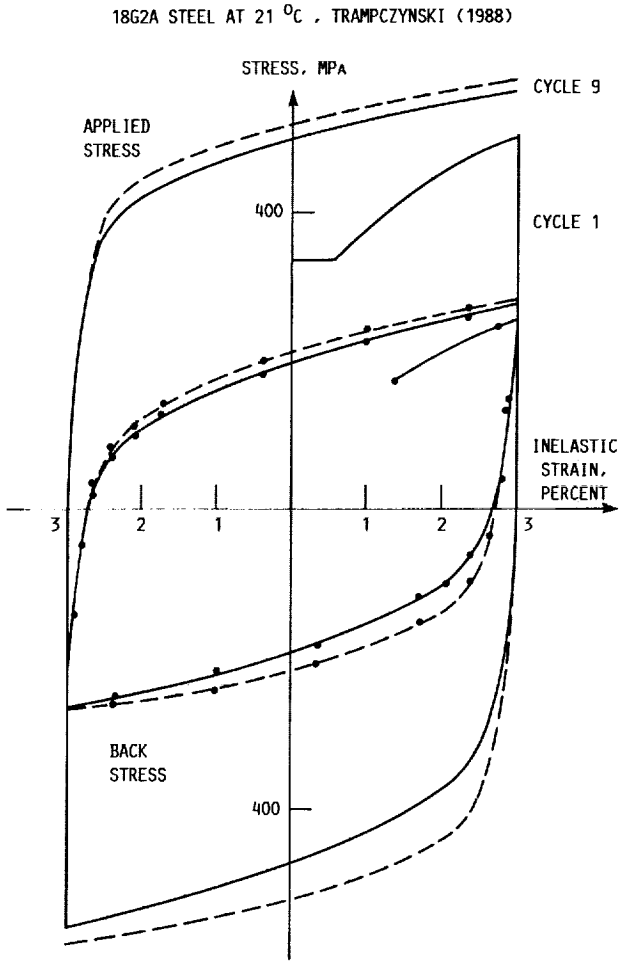

FIGURE 13. - STRESS AND BACK STRESS VERSUS INELASTIC STRAIN RESPONSE OF 18G2A STEEL AT ROOM TEMPERATURE. (DATA ARE FROM REF. 25).

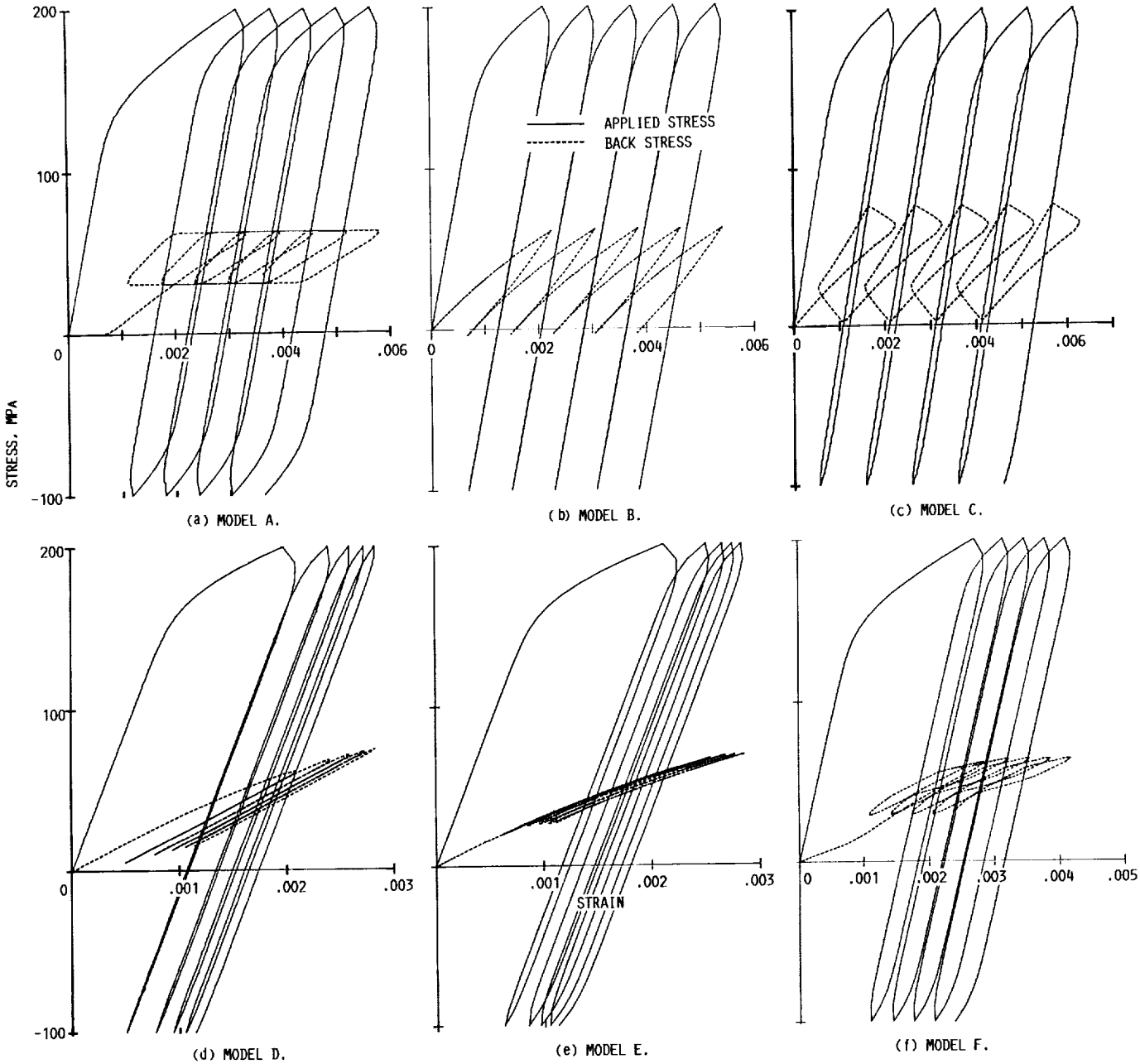

FIGURE 14. - COMPARISON OF RESULTS FOR A CLASSICAL RATCHETTING TEST.

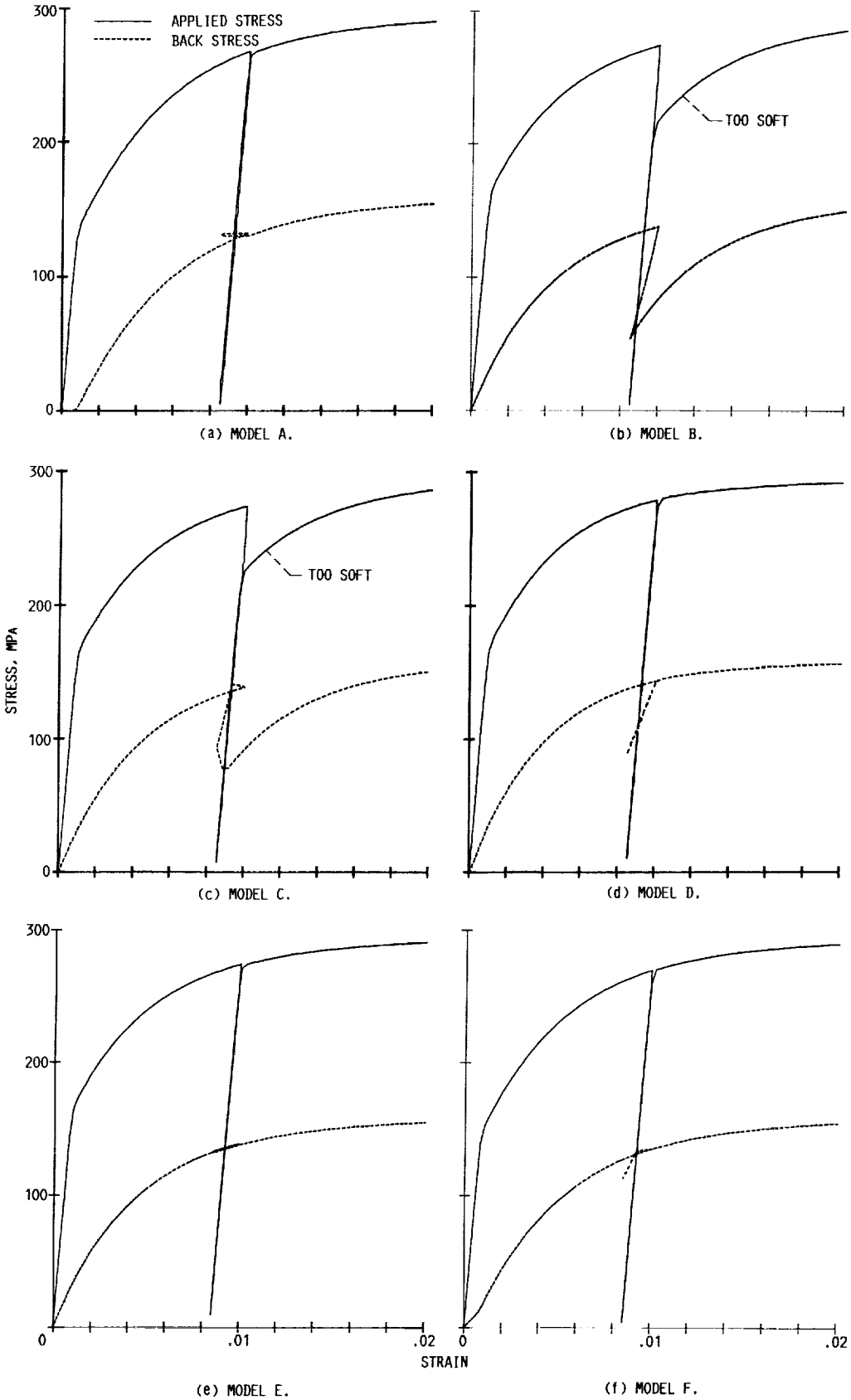

(a) MODEL A. (b) MODEL B.

(c) MODEL C. (d) MODEL D.

(e) MODEL E. (f) MODEL F.

FIGURE 15. - COMPARISON OF RESULTS FOR AN INTERRUPTED TENSILE TEST.

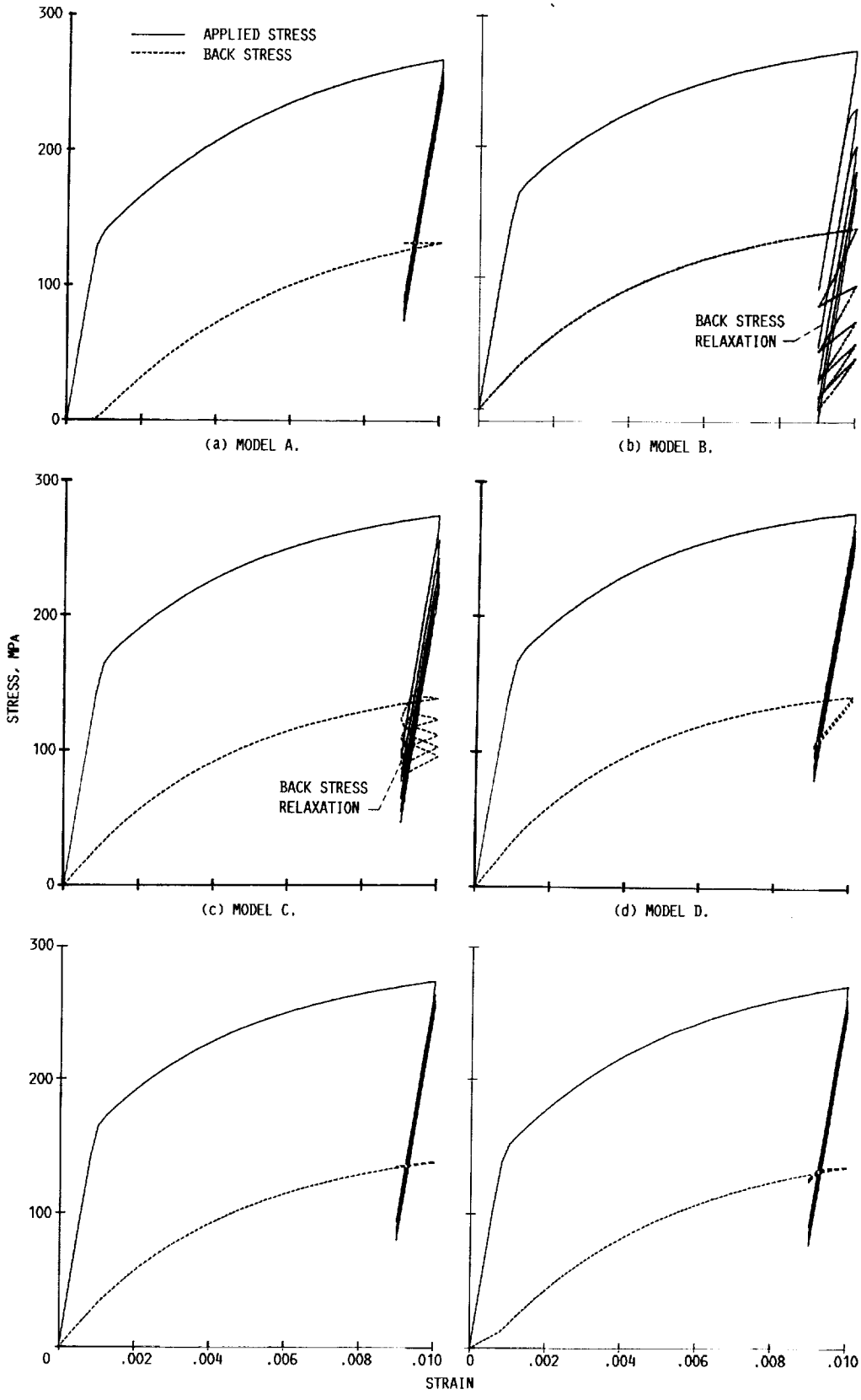

FIGURE 16. - COMPARISON OF RESULTS FOR AN ELASTIC RATCHETTING TEST.

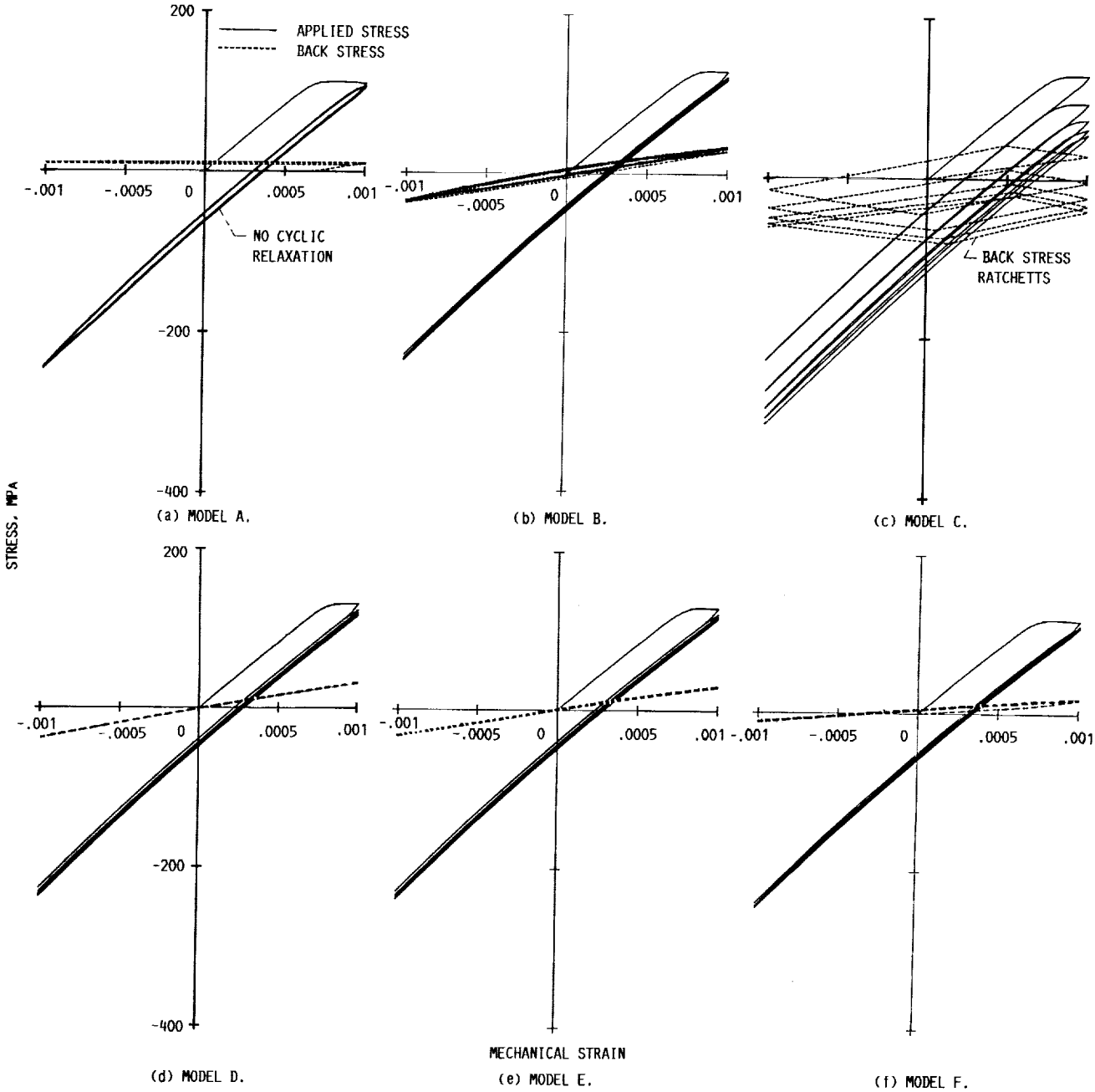

FIGURE 17. - COMPARISON OF RESULTS FOR A THERMOMECHANICAL FATIGUE TEST.

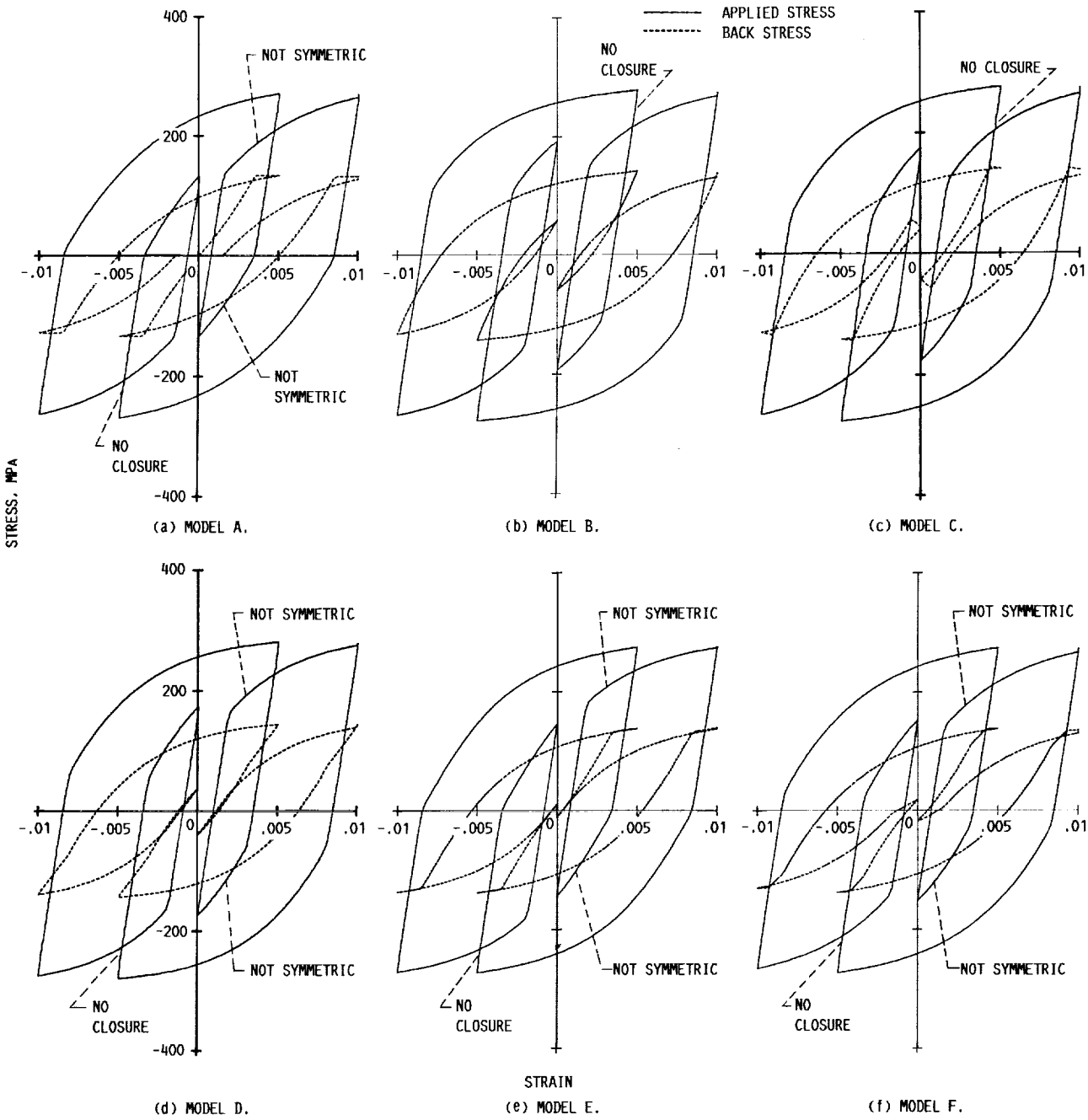

FIGURE 18. - COMPARISON OF RESULTS FOR A CYCLIC TEST.

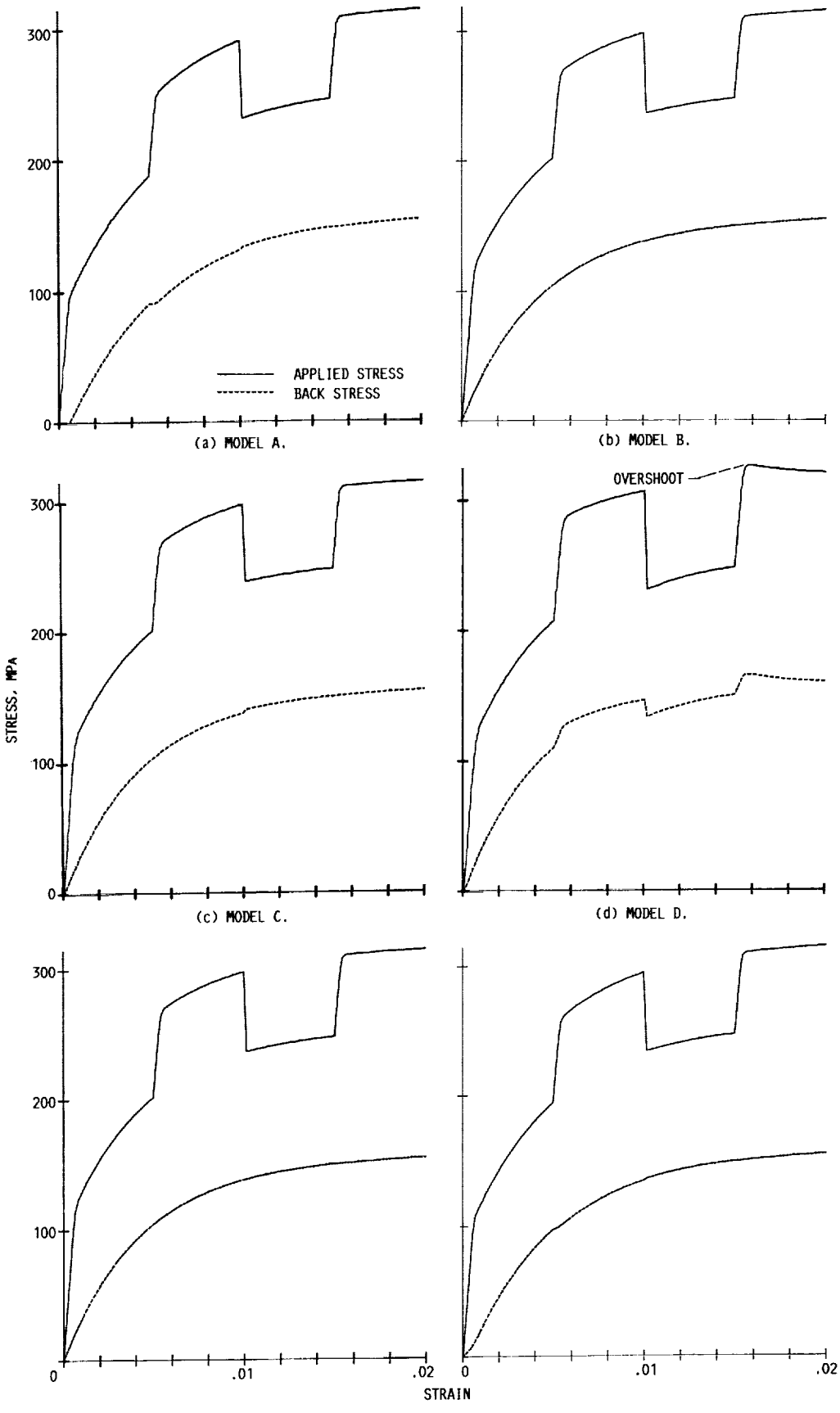

FIGURE 19. - COMPARISON OF RESULTS FOR A STRAIN-RATE JUMP TEST.

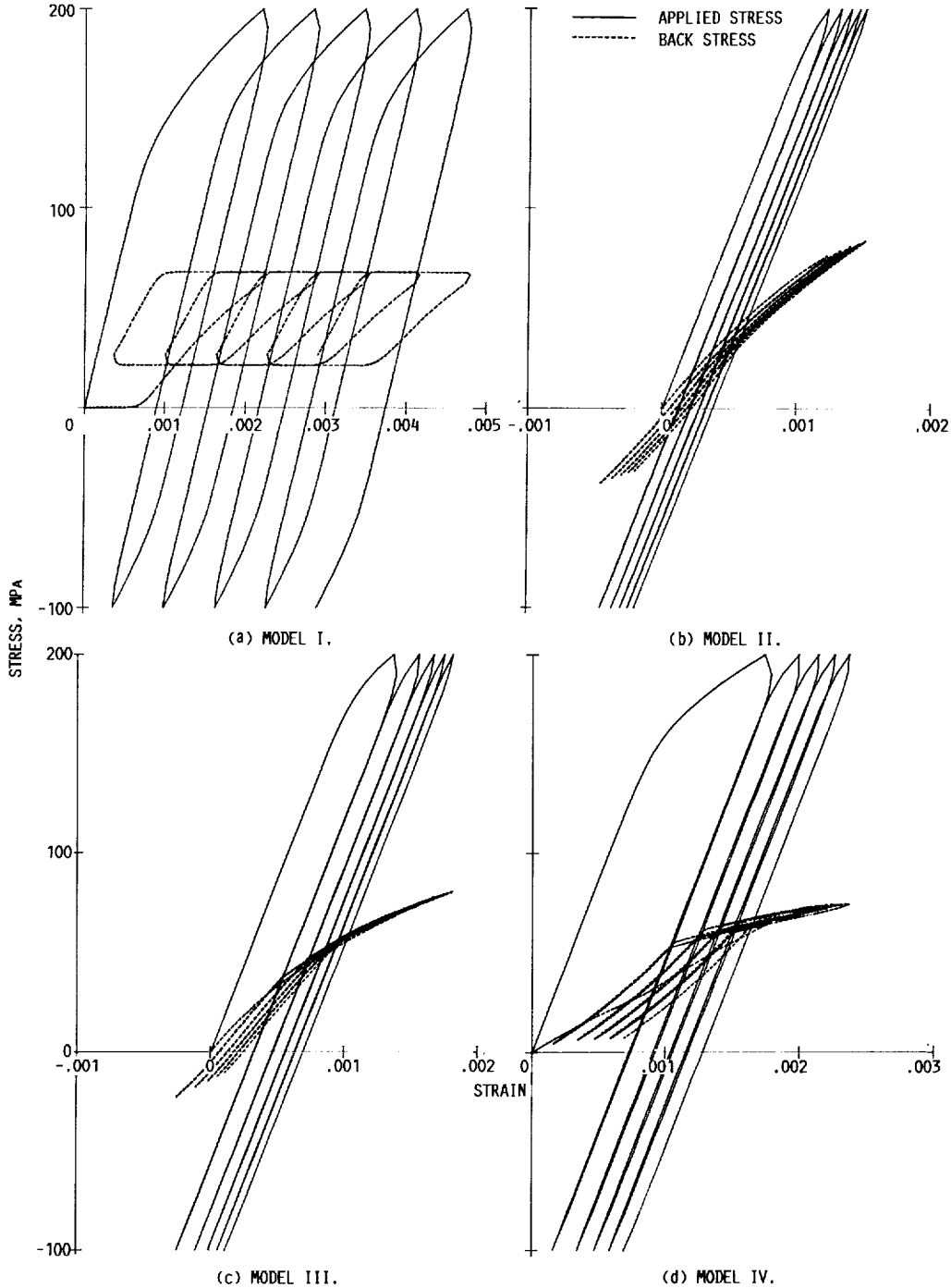

FIGURE 20. - COMPARISON OF RESULTS FOR A CLASSICAL RATCHETTING TEST.

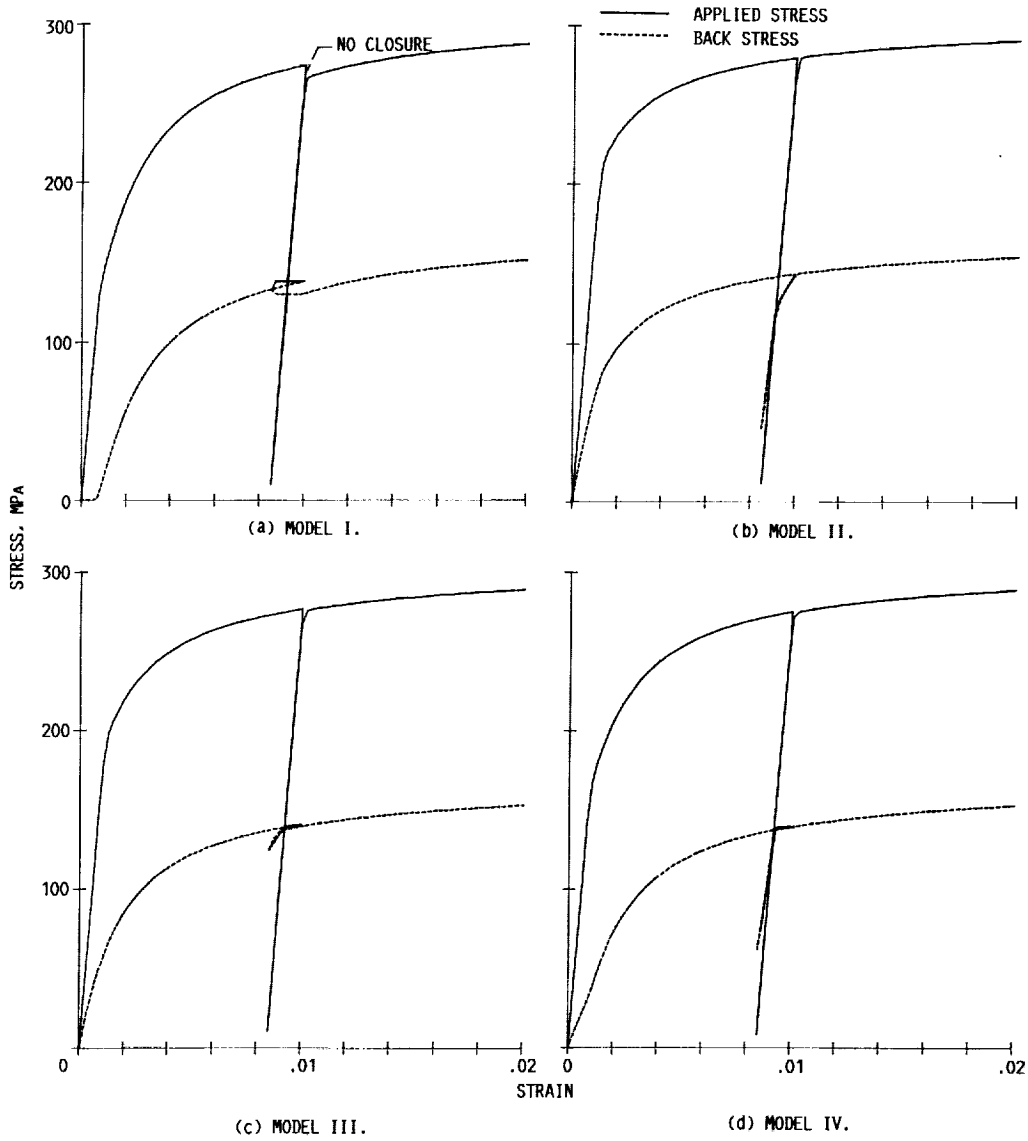

FIGURE 21. - COMPARISON OF RESULTS FOR AN INTERRUPTED TENSILE TEST.

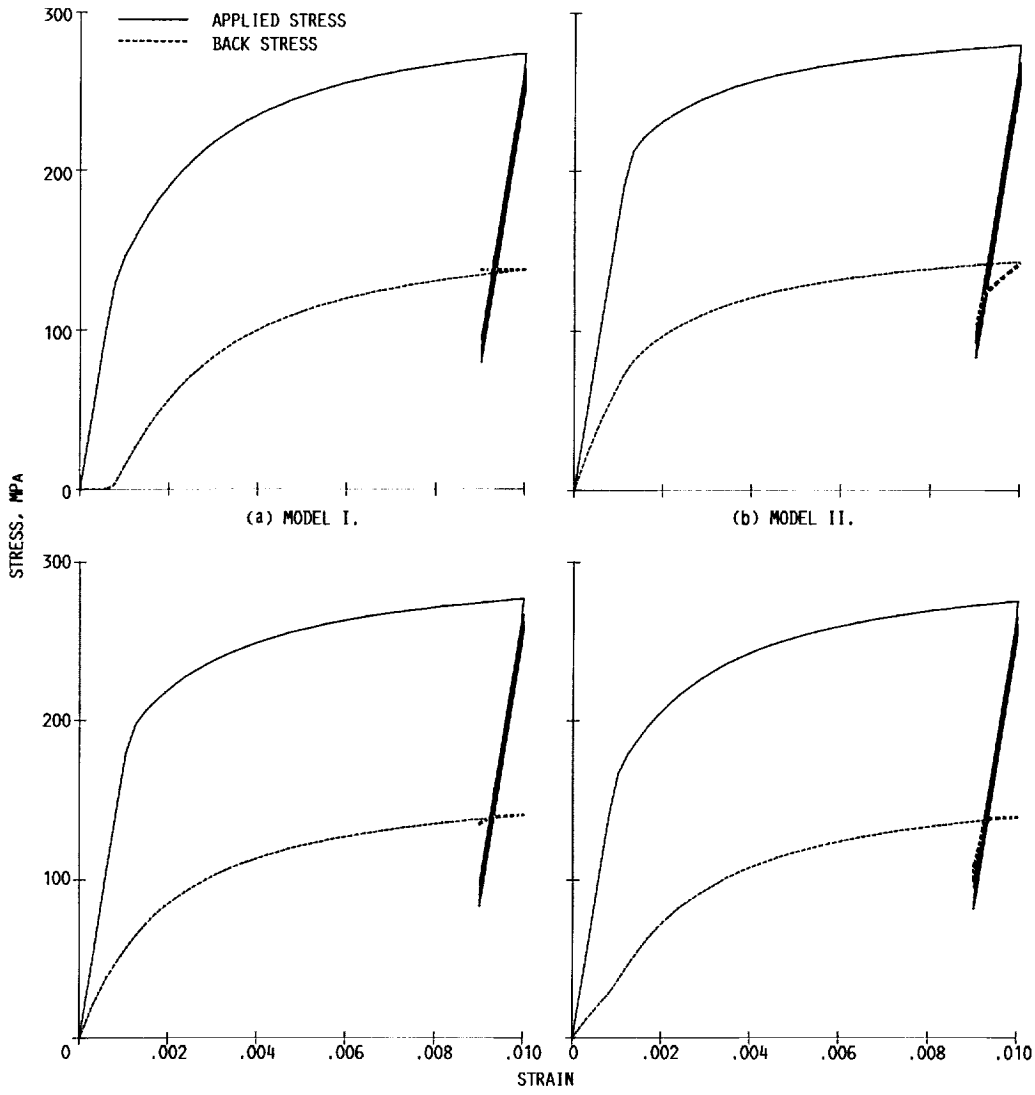

FIGURE 22. - COMPARISON OF RESULTS FOR AN ELASTIC RATCHETTING TEST.

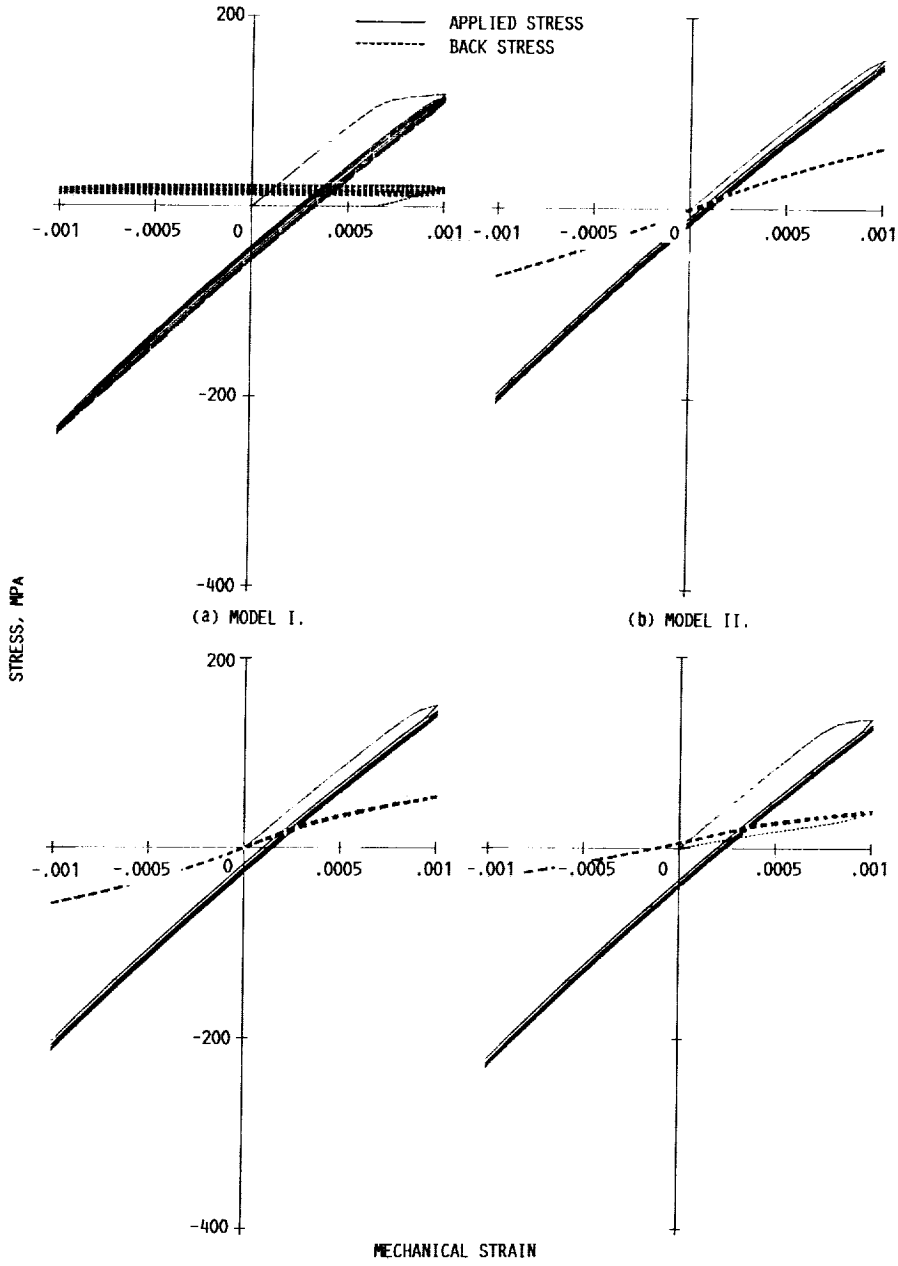

FIGURE 23. - COMPARISON OF RESULTS FOR A THERMOMECHANICAL FATIGUE TEST.

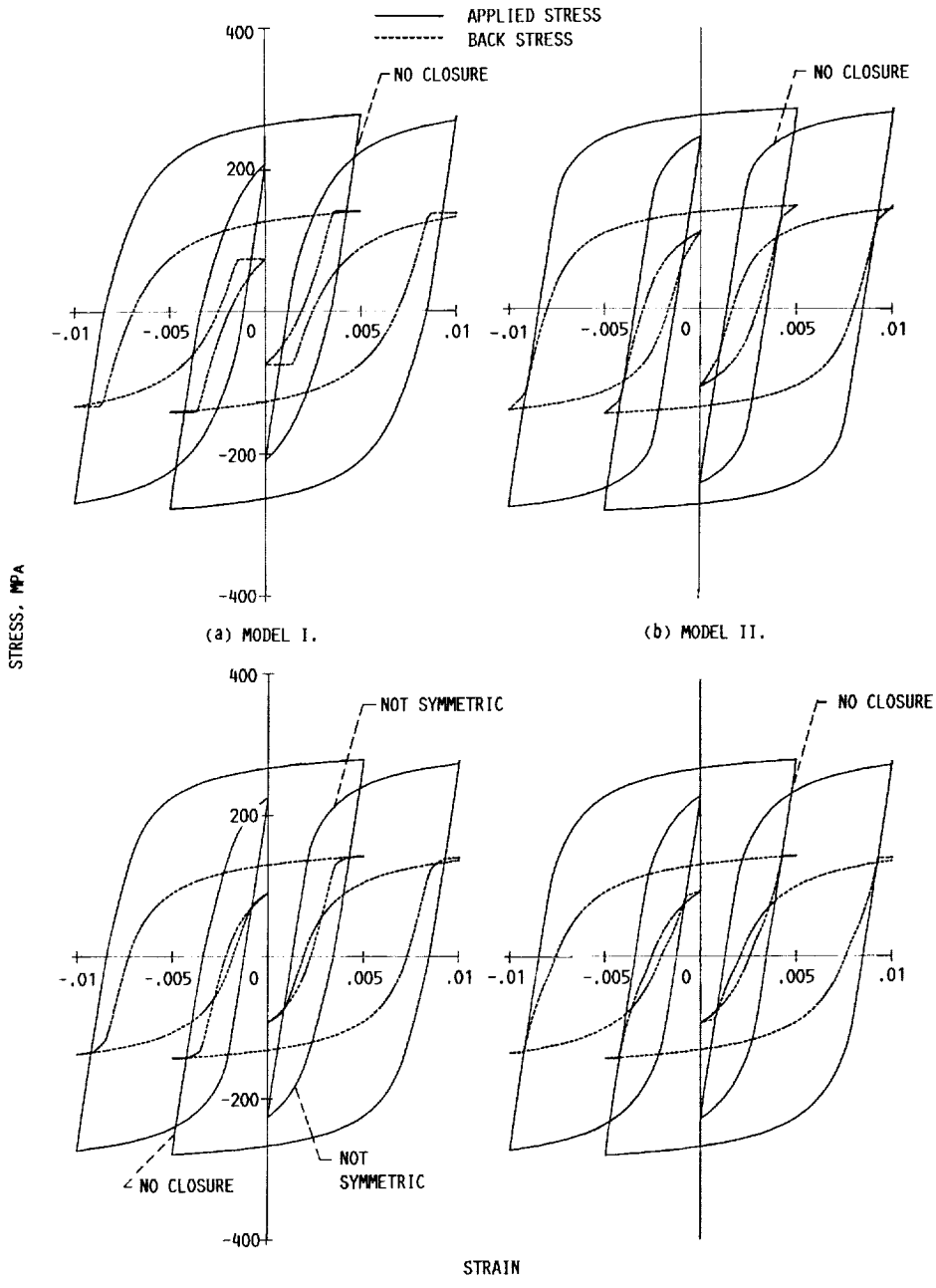

(a) MODEL I. (b) MODEL II.

(c) MODEL III. (d) MODEL IV

FIGURE 24. - COMPARISON OF RESULTS FOR A CYCLIC TEST.

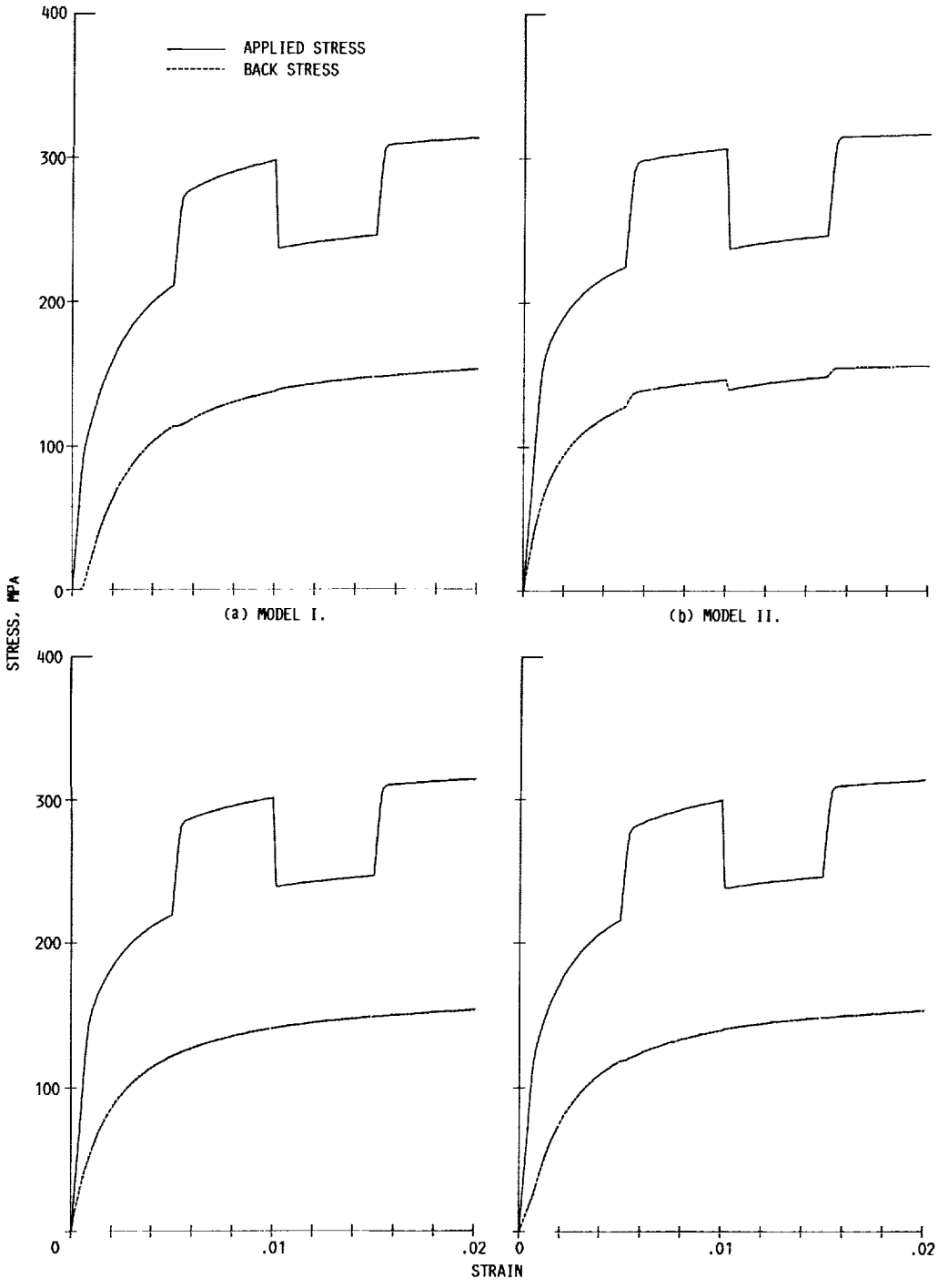

FIGURE 25. - COMPARISON OF RESULTS FOR A STRAIN-RATE JUMP TEST.

NASA
National Aeronautics and Space Administration

Report Documentation Page

1. Report No.	2. Government Accession No.	3. Recipient's Catalog No.
NASA TM-102509		

4. Title and Subtitle	5. Report Date
Model Development in Viscoplastic Ratchetting	April 1990
	6. Performing Organization Code

7. Author(s)	8. Performing Organization Report No.
Alan D. Freed and Kevin P. Walker	E-5311
	10. Work Unit No. 505-63-1B

9. Performing Organization Name and Address	11. Contract or Grant No.
National Aeronautics and Space Administration Lewis Research Center Cleveland, Ohio 44135-3191	
	13. Type of Report and Period Covered Technical Memorandum
12. Sponsoring Agency Name and Address	14. Sponsoring Agency Code
National Aeronautics and Space Administration Washington, D.C. 20546-0001	

15. Supplementary Notes

Alan D. Freed, NASA Lewis Research Center; Kevin P. Walker, Engineering Science Software, Inc., Smithfield, Rhode Island 02917.

16. Abstract

Space Station Freedom's solar dynamic power modules, like all power plants, contain components that are subjected to conditions which favor thermally driven ratchetting. Existing viscoplastic models tend to overpredict ratchetting behavior, because their back stress (the kinematic variable) seems to "stick" more than it should during unloading. For this reason, a study has been undertaken to compare a variety of possible modifications to the evolution equation for back stress. All models considered herein have a hardening *vs.* dynamic-recovery format. To remove the stickiness of the back stress, a linear dependence on stress rate is introduced into the evolution equation for back stress in a variety of ways. Several favorable models have been screened out of the field of candidates by qualitatively determining their relative ability to fit experimentally observed behavior through six numerical experiments. A final selection must be made by quantitatively correlating the proposed models with experimental data, and then seeing which candidate does the best job of predicting observed ratchetting behavior. This is a subject of future work.

17. Key Words (Suggested by Author(s))	18. Distribution Statement
Viscoplasticity Ratchetting Back stress	Unclassified – Unlimited Subject Category 39

19. Security Classif. (of this report)	20. Security Classif. (of this page)	21. No. of pages	22. Price*
Unclassified	Unclassified	32	A03

NASA FORM 1626 OCT 86

*For sale by the National Technical Information Service, Springfield, Virginia 22161